GEOLOGICA CARPATHICA, 2026, 77, 2, 163–185 https://doi.org/10.31577/GeolCarp.2026.07

A model for weathering of carbonate replacement deposits: Case study Petrova and Trgovska gora Mts., Dinarides, Croatia

SIBILA BOROJEVIĆ ŠOŠTARIĆ[1,✉], TENA KARAVIDOVIĆ[2], TOMISLAV BRENKO[1] and TAJANA SEKELJ IVANČANIN[2]

[1]University of Zagreb, Faculty of Mining, Geology and Petroleum Engineering, Pierottijeva 6, 10000 Zagreb, Croatia
[2]Institute of Archaeology, Jurjevska ulica 15, 10000 Zagreb, Croatia

(Manuscript received November 24, 2025; accepted in revised form March 18, 2026; Associate Editor: Igor Broska)

Abstract: An integrated mineralogical and geochemical study was conducted to evaluate links between carbonate replacement siderite–polysulphide (Cu, Pb, Ag±Ba) deposits, associated gossans, archaeological slag and distal bog-iron ores in the Trgovska Gora and Petrova Gora Mountains, Dinarides. A total of 45 samples were collected from ten mining sites located at hilly area (primary ore, proximal gossans, archaeological slag) and three lowland bog-iron occurrences up to 100 km away. Primary deposits and gossans are hosted by synorogenic flysch sequence, covered by soil and vegetation. Degree of weathering is high (median value of Chemical Alteration Index is 85 %). Petrographic analysis, X-ray diffraction, and multivariate geochemical analysis of major, trace, and rare-earth elements were used to reconstruct pathways of iron and base-metal mobilization. Results support three-stage weathering model for carbonate replacement deposits: (1) chemical weathering of primary siderite–polysulphide mineralisation and oxidation in vadose zone to goethite (hematite, lepidocrocite, dusty limonite)±malachite, azurite, anglesite, development of proximal (residual) gossan; (2) mechanical weathering and transportation of weathered Fe-ore (together with associated host-rocks) and its deposition as distal, reworked or pedogenical gossan, (3) chemical transportation of dissolved metals in saturated zone by reductive groundwater via gravitational flow to 50–100 km distance and reprecipitation in topsoil as bog-iron ore. Immobile trace elements (Zr, Nb, Ta, Hf, W), redox-sensitive elements (Mo, V, U), and REEs are consistently enriched in the aluminosilicate matrix and traceable from primary ore to gossans, bog iron, and slag. The persistent geochemical anomalies of Fe, Mn, Cu, Pb, Zn, Ag, Co, Ni, Sn, Sb, As, and Ba across all materials demonstrates inherited hydrothermal signature despite dilution in distal deposits.

Keywords: carbonate replacement deposits, gossan, bog iron ore, mineralogy, geochemistry, iron provenance, iron slag

Introduction

Carbonate-replacement deposits (CRD) are typical source of iron in circum-Pannonian region and have been in operations for centuries (Fig. 1A). Their origin and genesis are well constrained and summarised in literature (Boláček & Mihok 1994; Hofstra et al. 1999; Hurai et al. 2002; Radvanec et al. 2004; Palinkaš et al. 2008, 2016; Borojević Šoštarić et al. 2009; Strmić Palinkaš et al. 2009; Boch et al. 2018; Prochaska 2016; Németh et al. 2017; Neubauer et al. 2025 and references therein; Table 1):

- Carbonate replacement mineralisation is stratabound and almost exclusively linked with circum-Pannonian Silurian–Devonian carbonate belt (Silurian–Devonian olistoliths or carbonate intercalations of Carboniferous flysch within Dinarides; Devonian limestones/marbles in Alps; Silurian limestone belt including some Carbonifferous carbonate within Gemerides). Exception is Hungarian deposit Rudabánya, associated with Triassic carbonates.
- Most authors agree that formation model for origin of carbonate replacement deposits is hydrothermal-metasomatic.
- Circum-Pannonian carbonate replacement deposits are large to very large and hosts millions of tons of ore (Erzberg: 400 Mt; Ljubija: 350 Mt; Rudabánya 57 Mt; Hüttenberg: 50 Mt; Gemerides: 30 Mt).
- Host carbonate units are metamorphosed to various degree during Alpine orogeny events. Generally, Dinaric deposit (Ljubija, Trgovska and Petrova gora) show low to no metamorphic overprint, while Alpine (Erzberg, Hüttenberg) and Gemeride deposits as well as Rudabánya are metamorphosed to various degree (reaching amphibolite facies in Hüttenberg case). Age dating is shoving various Alpine stages, from Cretaceous to Miocene.
- Carbonate-replacement ore formation is followed by multistage hydrothermal overprints that introduce mainly siderite–quartz–sulphide polymetallic mineralisation. In Gemerides and Dinarides vein districts comprise hundreds of steeply dipping veins with significant vertical extent and pronounced

✉ corresponding author: Sibila Borojević Šoštarić
sibila.borojevic-sostaric@rgn.unizg.hr

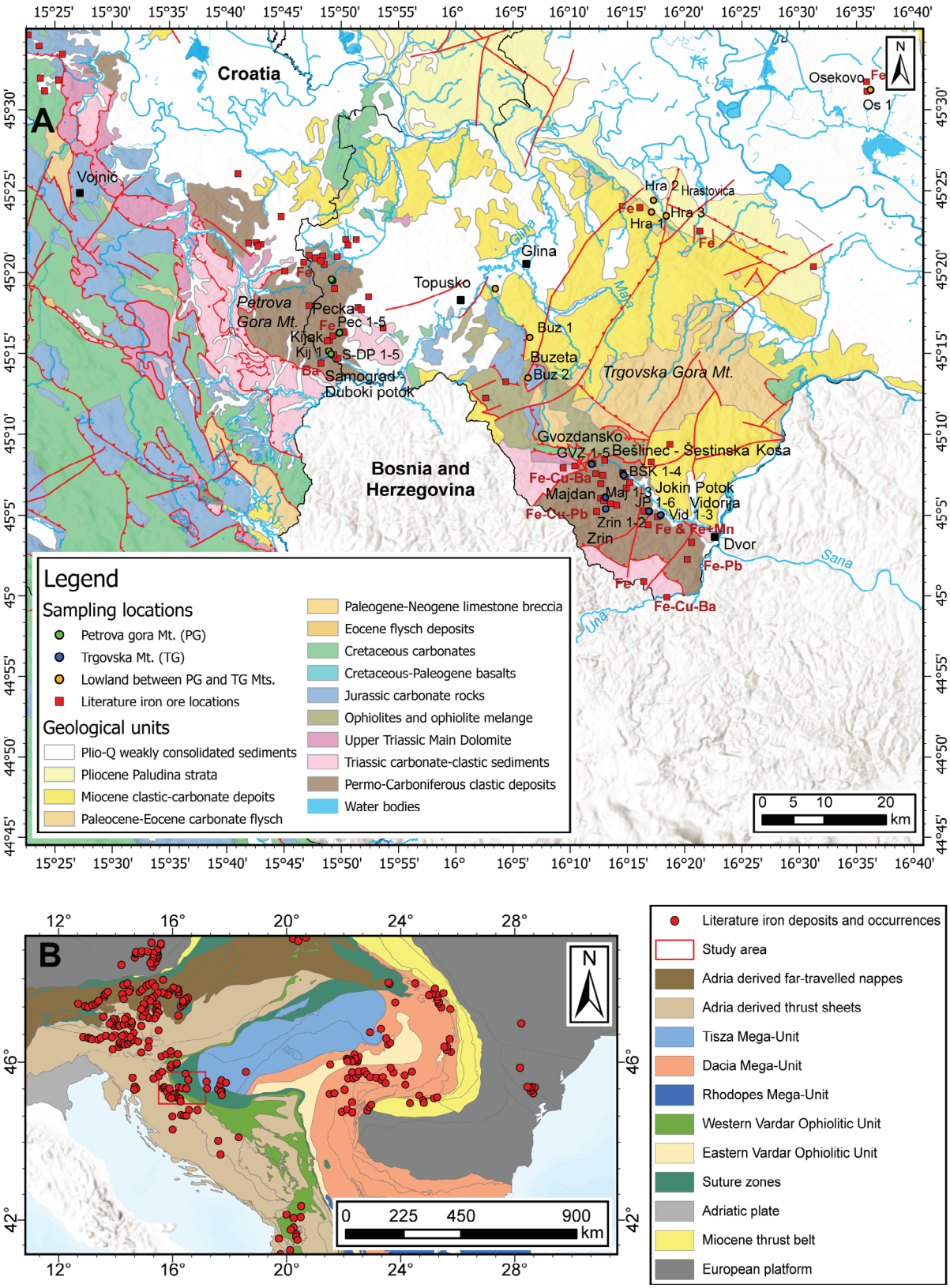

Fig. 1. Position and geological map of the study areas. **(A)** A geological map of the study area with sampling locations from Petrova and Trgovska Mts. and surrounding low-terrain areas and literature locations of iron ore occurrences and historical mining activity (according to Jurković 1962; Šikić et al. 1979; Marković 2002; Velić & Vlahović 2009). **(B)** Simplified geological map of circum-Pannonian area with basic geological features, red square showing study area map at Central Croatian (after Schmid et al. 2020).

Table 1: Carbonate replacement deposits in circum-Pannonian region.

Terrain	Deposit	Reserves (Mt)	Age of the host rock	Mineralization type	Degree of metamorphism	Age of metamorphic overprint	References
Alps	Erzberg	400	Devonian limestones/ marbles	Stratabound	Greenschist facies	Hercinian–Cretaceous	Prochaska 2016; Boch et al. 2018
	Huttenberg	50	Devonian marble	Stratabound	Amphibolite facies	Cretaceous–Miocene	Neubauer et al. 2025
Dinarides	Ljubija	350	Silurian–Devonian olistoliths within Carboniferous flysch	Stratabound	Anchimetamorphism	Very weak Cretaceous	Palinkaš et al. 2008, 2016; Strmić Palinkaš et al. 2009
	Trgovska gora	1	Carboniferous–early Permian flysch	Stratabound, vein type	Anchimetamorphism	Very weak Cretaceous	Borojević Šoštarić et al. 2009; Palinkaš et al. 2008, 2016
	Petrova gora	<0.5	Carboniferous–early Permian flysch	Vein type	No metamorphism	No record	Borojević Šoštarić et al. 2009; Palinkaš et al. 2008, 2016
Gemerides	Numerous deposits	80	Silurian limestone belt, minor Carboniferous	Stratabound, vein type	Anchimetamorphism-greenshists facies	Cretaceous	Boláček & Mihok 1994; Radvanec et al. 2004; Hurai et al. 2002
Carpathians	Rudabánya	57	Triassic	Stratabound	No metamorphism	No record	Hofstra et al. 1999; Németh et al. 2017

zoning, and significant reserves (Gemerides >50 Mt of ore is located within vein type of mineralisation). It is generally considered that polymetallic mineralisation is metamorphogenic in character and linked to various stages of the Alpine orogeny.

However, weathering of carbonate replacement deposits remains poorly understood compared to the weathering of primary sulphide deposits (i.e. SEDEX, VMS, Cu-porphyry; sensu Emmons 1917; Taylor et al. 1980; Andrew 1984; Thornber 1985; Butt & Zeegers 1992; Taylor & Thornber 1992; Boyle 1994; Butt et al. 2005, 2008). When uplifted and exposed, pyrite-rich sulphide deposits undergo oxidation above the water table forming gossans, while leaching and reprecipitation below the water table mobilise metals and redeposit them locally or distally as secondary ore, including bog iron (Blain & Andrews 1977; Taylor & Thornber 1992; Velasco et al. 2013). In the case of carbonate-replacement deposits, a link between primary iron ore, gossans and distal bog-iron ore deposits was never explored.

This study is a first attempt to investigate the mineralogical and geochemical relations between host rocks, primary ores, gossans and bog iron ore within weathered carbonate-replacement deposits. Study was conducted at two historical Croatian siderite–polysulphide mining areas: Petrova Gora and Trgovska Gora (PG and TG, respectively), located within the Variscan units of Dinarides. Mining activity in these areas is presumed to have begun in pre-Roman or Roman times (Jurković 1962; Jurković & Durn 1998; Durman 2002; Karavidović & Drnić 2022) and continued intermittently through historical periods until the 1960s (Marković 2002; Borojević Šoštarić et al. 2009). Historical records indicate that limonite-rich siderite ores contained up to 60 wt% Fe, comparable to contemporary iron ore grades, while copper contents in Trgovska Gora ores (6.5–8.0 wt%) exceeded typical contemporary grades by a factor of 6–7, while galena-rich ores hosted 33–280 ppm Ag (Jurković 1958). The total extraction of mineral resources from the region is estimated to exceed 1 Mt of iron ore, predominantly from oxidation zones, in addition to several thousand tonnes of Cu, 2000–3000 t of Pb, and 800–1400 t of Ag (Jurković 1962; Marković 2002).

The objectives of this study are to address: (1) geological and metallogenic characteristics of the regions; (2) the mineralogy, petrography and geochemistry of the host rocks and primary hydrothermal siderite–polysulphide mineralisation; (3) the mineralogy, petrography and geochemistry of the secondary proximal and distal iron-mineralisation; (4) the geochemical link between primary and secondary mineralisation and archaeological slag.

Geological setting

Circum-Pannonian CRD

The largest European siderite deposit, Erzberg in the Eastern Alps, is hosted in Devonian limestones and marbles of the Greywacke Zone and has produced ~245 Mt of iron ore, with an additional ~150 Mt in remaining reserves, bringing its total endowment to ~400 Mt (Prochaska 2016). Its siderite–ankerite mineralisation, accompanied by calcite, quartz, muscovite/sericite and accessory sulphides, reflects a complex Variscan to Alpine tectonothermal evolution, while young erzbergite laminated ore formed through meteoric water infiltration and sulphide oxidation that mobilised Ca–Mg–Fe from the host rocks (Boch et al. 2018). The second largest accumulation, the Ljubija iron-ore district in the Dinarides (~350 Mt), comprises stratabound, carbonate-replacement siderite–ankerite bodies and hydrothermal siderite–polysulphide veins formed within a Silurian–Devonian olistoliths and Carboniferous flysch (Palinkaš et al. 2008; Borojević Šoštarić et al. 2009; Strmić Palinkaš et al. 2009). Ore formation involved medium-temperature basinal brines, with Permian seawater providing sulphur for baryte and sulphides, and temperatures constrained by isotope and fluid inclusion data to 164–224 °C.

Other major CRD deposits include Rudabánya in Hungary (~57 Mt) a carbonate replacement deposit located within Triassic carbonates and accompanied by polymetallic sulphide mineralizaton (Németh et al. 2017), the Hüttenberg deposit in Austria (~50 Mt), hosted in Devonian marbles metamorphosed at 600–650 °C and ~0.1 GPa during the Eoalpine orogeny, with ore formation broadly postdating Cretaceous peak metamorphism (Schulz & Schroll 1997; Faryad & Hoinkes 2003; Pfingstl et al. 2015), and the siderite–polysulphide vein and metasomatic siderite–ankerite systems of the Gemeric Unit in the Western Carpathians (~80 Mt), formed predominantly during Variscan low-pressure metamorphism and driven by deep circulation of saline brines with only minor Alpine overprint (Boláček & Mihok 1994; Hurai et al. 2002; Radvanec et al. 2004).

Trgovska and Petrova gora Mts.

The Trgovska and Petrova gora Mts. represents a part of the pre-Mesozoic basement adjacent to the external, Pre-Karst unit of the Dinarides (sensu Schmid et al. 2020), correlated with the Sana-Una and Mid-Bosnian Schist Mountains (Hrvatović 2000; Hrvatović & Pamić 2005; Fig. 1B). The Pre-Karst unit is considered transitional between the carbonate platform units of the Adriatic (High Karst and the Dalmatian Zone) and the more internal Flysch Bosniaque, which marks the passive continental margin of the Dinarides, mainly consisting of distal platform-slope facies.

Petrova Gora (PG) comprises non-metamorphosed sedimentary sequences, while Trgovska Gora (TG) and the adjacent Sana-Una Paleozoic units underwent low-grade metamorphism, with localised higher metamorphism near tectonic zones. Inherited detrital white mica ages were obtained in both regions, ranging from 313.5±3.0 Ma to 353.8±4.2 Ma, with several younger tectono-thermal overprints (Borojević Šoštarić et al. 2009, 2012).

The central part of PG and TG consists of a pre-Mesozoic synorogenic flysch sequence, starting with fine-grained Early–Middle Carboniferous sediments, grading upward to Late Carboniferous–Early (Middle?) Permian quartz sandstones and conglomerates. An older, fine-grained sequence is composed of clayey to silty shales, sometimes interbedded with silty subgraywacke sandstones and siltites, grading to a younger, medium-to coarse-grained sequence composed of subgraywackes interbedded with clayey siltstones or shales interlayered with fine- to coarse-grained greywacke, sandstone, and minor fine-grained conglomerates in the upper section (Đurđanović 1968, 1973; Korolija et al. 1981). Carbonate intercalations/matrix is present within TG. The silty shales, clayey siltstones, as well as subgraywacke and sandstones, have similar mineralogical composition: detrital quartz fragments prevail, followed by sericite/muscovite, chlorite, feldspar, rock fragments, and opaque minerals/coalified matter within a sericite–clayey matrix, which also includes rutile, quartz, and carbonates (Jurković 1958; Đurđanović 1968, 1973).

Carboniferous–Permian deposits are thrust towards the SW, onto the Lower–Middle Triassic marine carbonate and siliciclastic sediments of the Adriatic carbonate platform, and are overthrust by Western Vardar Cretaceous–Paleogene ophiolites and flysch, occasionally intercalated with Scaglia-type limestones (Korolija et al. 1981; Schmid et al. 2020; Fig. 1B). Younger Pliocene and Quaternary sediments, composed of unconsolidated sands, clays, alluvial and fluvial deposits, and bog iron, are found in the areas of lower elevation (northern and eastern flanks), and as infill of fluvial valleys, reflecting the main erosional direction of TG and PG.

Mineralisation

Both TG and PG mineralisation are hosted within flysch. Within the TG, Fe-mineralisation is of carbonate replacement and vein type. The mineralisation is situated in a NE–SW trending zone, 16 km long and 7 km wide. Weak metal zonation is recognisable (Jurković 1959, 1988; Jurković & Durn 1988). The central part of the TG is Fe (Cu) rich, containing chalcopyrite, and is surrounded by an Fe (Pb, Ag) zone with Ag-galena and a broad Fe zone. The Fe-rich external zone consists of siderite–ankerite–quartz metasomatic ore layers and lenses developed within carbonate intercalations of the flysch sediments, containing up to 35 wt% Fe with 1–2 wt% sulphides. The primary iron ore is accompanied by various Fe-alteration products (hematite and limonite) ±Cu–Pb–Ag sulphides and, in rare cases, Ni–Co–As–Sb sulphosalts or cassiterite, and sometimes appears as irregular nests. Generally, early-stage quartz and sulphides (Ag-bearing galena, quartz, chalcopyrite, sphalerite, and pyrite) are succeeded by main-stage siderite and late-stage sulphides and complex sulphonates. The siderite is often Mg-rich, contains traces of Mn, Ca, and Sr, and is weathered via an irregular network of limonite veinlets.

The mineralisation of the PG Mt. consists of two zones: (i) the northwesternmost siderite-quartz-polysulphide, and (ii) southern baryte zone. The siderite–quartz–polysulphide zone is 7 km long and 4 km wide, while baryte zone is 6 km long and 0.7 km wide. Mineral succession includes early siderite, quartz, pyrite, chalcopyrite, and sphalerite, respectively. Within the baryte zone, early baryte is followed by siderite, pyrite, quartz, chalcopyrite, and tetrahedrite. Both zones consist of vein-type mineralisation, striking NE–SW, dipping toward the NW, with average thicknesses between 0.5 and 7 m. Maximum length of veins is 250 m, while the vertical extent of mining reaches 60 m (Marković 2002). Veins are surrounded by cm–dm thick alteration zones, typically sericitized, silicified, and sideritized (often limonitized).

Materials and methods

Field survey and sampling

A total of 29 samples were collected from the Trgovska Gora area (Supplementary Table S1; Figs. 1A, 2A–D). Various

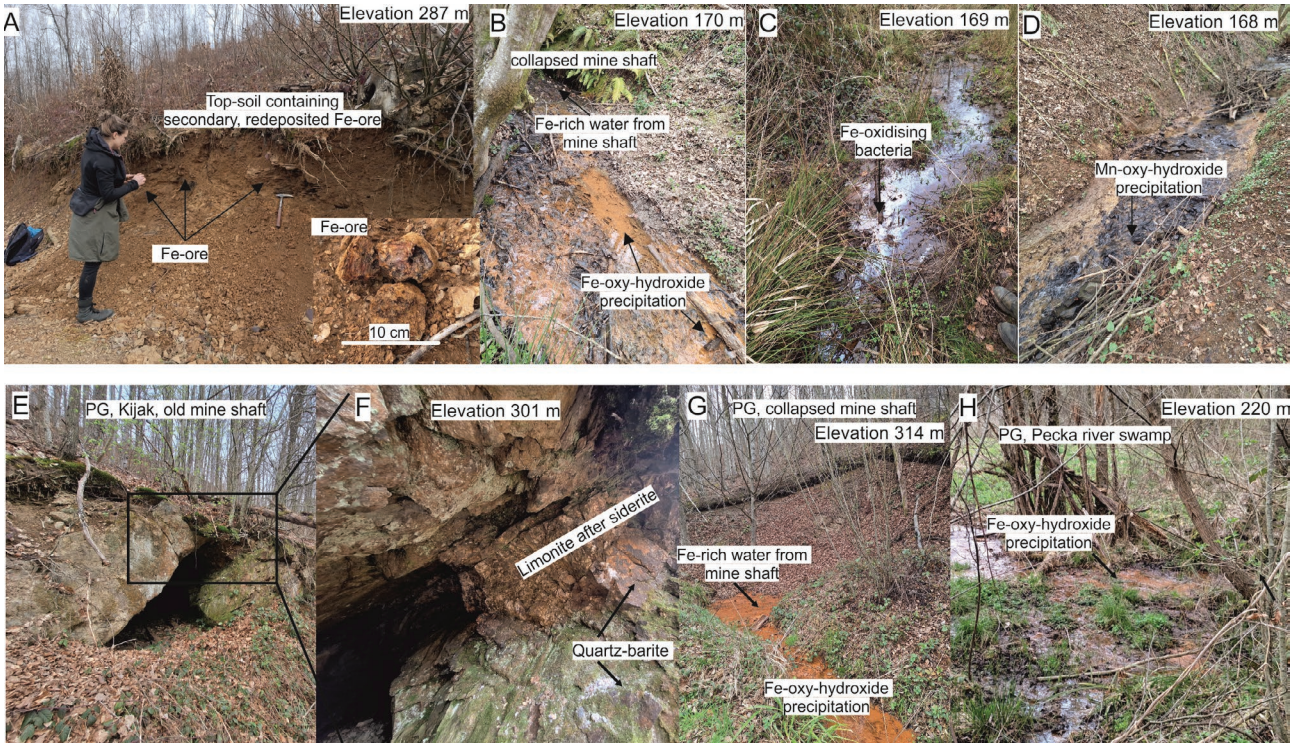

Fig. 2. (A–D) Field photographs of the TG outcrops. A – Majdan locality: redeposited primary mineralisation in the soil profile (40–70 cm depts; 287 m a.s.l.); B–D – Jokin potok locality; B – Fe-oxyhydroxide precipitate from water draining old mining shaft; C – Fe-oxidising bacteria on the surface of creek water; D – Mn-oxyhydroxide precipitate from creek below mining old damp. **(E–H)** Field photographs of the PG outcrops; E, F – Kijak locality, old mine shaft with siderite–goethite–baryte ore within limonitised sandstone; G – Pecka locality (314 m a.s.l.), Fe-oxyhydroxide precipitate from water draining old mining shaft; H – Pecka river swamp (220 m a.s.l.), with Fe-oxyhydroxide precipitation.

altered siderite–hematite–sulphide metasomatised/vein-type mineralisation and limonitised/hematitised sandstone and conglomerate were sampled at Gvozdansko, Bešlinec, Zrin, Jokin Potok, and Vidorija. Observations at the collapsed adit and creek drainage (yellow water, Fe–Mn oxyhydroxide precipitates, Fe-oxidising bacterial films) indicate mine drainage (Fig. 2B–D). Goethite–limonite ores proximal to primary deposits were sampled at Bešlinec, Majdan, and Jokin Potok. At Majdan, mechanically eroded and chemically weathered primary ores were identified in soil at 40–70 cm depth beneath a waterlogged, swamp-vegetated area (Fig. 2A). A bloomery tap slag sample from Jokin Potok, found on a mine dump, provides the first tangible evidence of historical iron production at Trgovska Gora.

From the hilly part of Petrova Gora Mt., a total of 13 samples were collected (Supplementary Table S1; Fig. 2E–H). They include primary Fe–Ba mineralisation, composed of altered siderite–goethite–quartz vein-type mineralisation and limonitised/hematitised sandstone and conglomerate rocks, collected from the locations Petrovac and Pecka. Location Kijak was underground mine shaft with siderite–goethite–baryte ore within limonitised sandstone (Fig. 2E, F). No proximally developed secondary ore was found in the Petrova Gora area; however, waterlogged valleys of streams flowing towards the Pecka river, as well as swampy areas surrounding the Pecka river, showed evidence of mine drainage (yellow stream water, Fe-oxyhydroxide at the creek floor; Fig. 2G, H).

The lowland area between the Petrova and Trgovska gora Mts. was studied for secondary, distal bog-iron goethite–limonite ore occurrences. Goethite–limonite nodules and concretions (0.5–5 cm in diameter) were collected from the topsoil (0–20 cm) and along the stream banks in the lowland between the Petrova and Trgovska gora regions, at the locations of Osekovo, Hrastovica, and Buzeta (Supplementary Table S1).

Laboratory analyses and data processing

Micropetrographical study was performed on weakly-moderately altered primary and proximal secondary iron-ore mineralisation, distal secondary lowland ore as well as archaeological slag (Supplementary Table S1). Microphotographs were taken using an OPTIKA B-1000 microscope with 5×, 10×, and 20× magnification, OPTIKA C-P6 FL camera, and OPTIKA ProView software.

Twenty-two moderately to heavily altered iron-ore samples from TG, eight from PG, three from the lowland area, and one iron-slag sample (Table 1) were analysed mineralogically at the University of Zagreb Faculty of Mining, Geology and Petroleum Engineering. Between 300 and 500 grams of bulk samples were crushed and passed through a 2 mm sieve. They

were then ground to obtain the powdered fraction. The powdered samples were analysed by X-ray powder diffraction using a Malvern Panalytical Empyrean diffractometer equipped with 0.5° divergent and anti-scatter slits, 0.03 and 0.04 rad soller slits, Cu-Kα radiation, operated at 45 kV and 40 mA with a PIXcel 3D detector, while data acquisition was conducted with a step size of 0.0130 °2θ. The mineral phases in the samples were identified using PANalytical X'Pert HighScore 5.2.0 software, with standard Powder Diffraction Files (PDF) from the International Centre for Diffraction Data (ICDD). Semi-quantitative analysis was performed using the Rietveld refinement function integrated in the X'Pert HighScore software, referencing crystallographic data from the Crystallography Open Database (COD) (Vaitkus et al. 2023).

Detailed geochemical analyses of selected samples, including major, trace and rare earth element (REE) contents, was determined by Bureau Veritas laboratory in Krakow, Poland (Supplementary Table S2). A total of 18 moderately-heavily altered primary and secondary iron-ore samples from TG, eight variably altered samples from PG, three samples from lowland between TG and PG, and one TG iron slag were selected. Major element oxide contents were determined using X-ray fluorescence analysis on fused discs. Trace and rare earth elements contents were determined using a combination of inductively coupled plasma mass spectrometry (ICP-MS), after 4-acid digestion (near-total digestion) for trace elements or after lithium borate fusion in case of rare earth elements. Four internal standards and numerous blanks were utilized during the analyses, ensuring instrumental precision between 3 and 5 %, and detection limits for all elements in ppm or lower.

Statistical analysis was performed in TIBCO Statistica 14.0. Multivariate chemometric methods were used as the primary statistical approach to observe the relationships between analysed samples, specifically Principal Component Analysis (PCA) and Hierarchical Cluster Analysis (HCA), followed by other explanatory methods on selected samples. Results of chemical analyses were standardised for multivariate (PCA and HCA) analysis using the z-score to ensure that each variable was equally weighted (Supplementary Tables S3, S4). Some samples contained elements with values below detection limits. The representation of these elements was taken as half of the detection limit for each element, according to the calibration used. HCA was performed using Ward's linkage method in combination with Euclidean distance as the dissimilarity measure.

The degree of chemical weathering of the studied samples was calculated using the Chemical Index of Alteration (Nesbitt & Young 1982, 1984). Major oxides were recalculated to moles, and CIA was determined using the formula:

$$[Al_2O_3/(Al_2O_3+CaO^*+Na_2O+K_2O)]\times 100$$

where high CIA values indicate a greater degree of chemical weathering, due to the effective removal of Ca^{2+}, Na^{+}, and K^{+} from the host rocks, compared to Al^{3+} and Ti^{4+}, which are more stable, and vice versa.

Results

Mineralogy and petrology

Trgovska Gora

Host rocks and primary hydrothermal Fe (Cu, Pb) mineralisation:

Iron-rich mineralisation at Trgovska Gora occurs mainly as veins and veinlets within fine- to coarse-grained sandstone, greywacke (Fig. 3A, and conglomerate rocks. Locally, clast-supported ore breccias is also present (Fig. 3B). Moderately to heavily altered rocks are highly porous, dominated by limonite with minor colloform goethite and only trace occurrences of quartz (Fig. 3C, D).

Mineralised greywacke and sandstone consist mainly of angular quartzite clasts and fine quartz fragments with elongated detrital muscovite (Fig. 4A). Dissolved or altered siderite is typically replaced by limonite, goethite or hematite. Pressure shadows composed of fibrous quartz or muscovite with opaque minerals are common (Fig. 4A). The fine-grained matrix consists of sericite, quartz, siderite and opaque minerals, crosscut by similar veinlets or cemented by medium-grained siderite, partly limonitised. Veins contain coarse-grained siderite (partly or fully hematitised), quartz and titanium minerals (titanite–rutile), indicating multiple stages of vein formation. Conglomerate rocks show similar textures with rounded quartzite clasts up to 5×6 mm that are embedded in a quartz–sericite–opaque matrix and decorated with pressure shadows. Mineralisation surrounds clasts and appears as cataclastic flow. Veinlets less than 1 mm wide with limonitised opaque minerals and disintegrated quartz fragments are common.

Heavily altered sandstone/conglomerate containing more than 50 wt% goethite were analysed using XRD (Table 2). Goethite and quartz predominate, with illite–sericite (10 Å), sporadic clay minerals (7 Å and 14 Å), chlorite, rutile, Mn-minerals (todorokite?), lepidocrocite and ore minerals including hematite (especially at Vidorija), siderite, pyrite, sphalerite, galena, molybdenite and arsenopyrite.

Clast-supported ore breccia consists of angular to weakly rounded quartzite clasts, partly recrystallised with undulose extinction and pressure shadows of fibrous quartz/muscovite and siderite (partially limonitised). Fragments of greywacke or conglomerate preserve quartz and detrital muscovite. Fragments are embedded in a quartz–sericite–siderite matrix with limonitisation and hematitisation (Fig. 4C) or are cut by veinlets less than 1 mm thick containing hematite or limonitised siderite. Some veinlets contain fibrous muscovite, quartz and ore minerals. Large siderite crystals (several mm) are partially transformed to hematite or limonite and decorated with sericite–quartz pressure shadows. Cavities are common.

Brecciated samples from Gvozdansko were grouped by weathering ratio (limonite vs. siderite/ankerite). XRD shows an inverse relationship between goethite and gangue minerals (quartz±illite–smectite–chlorite; Table 1).

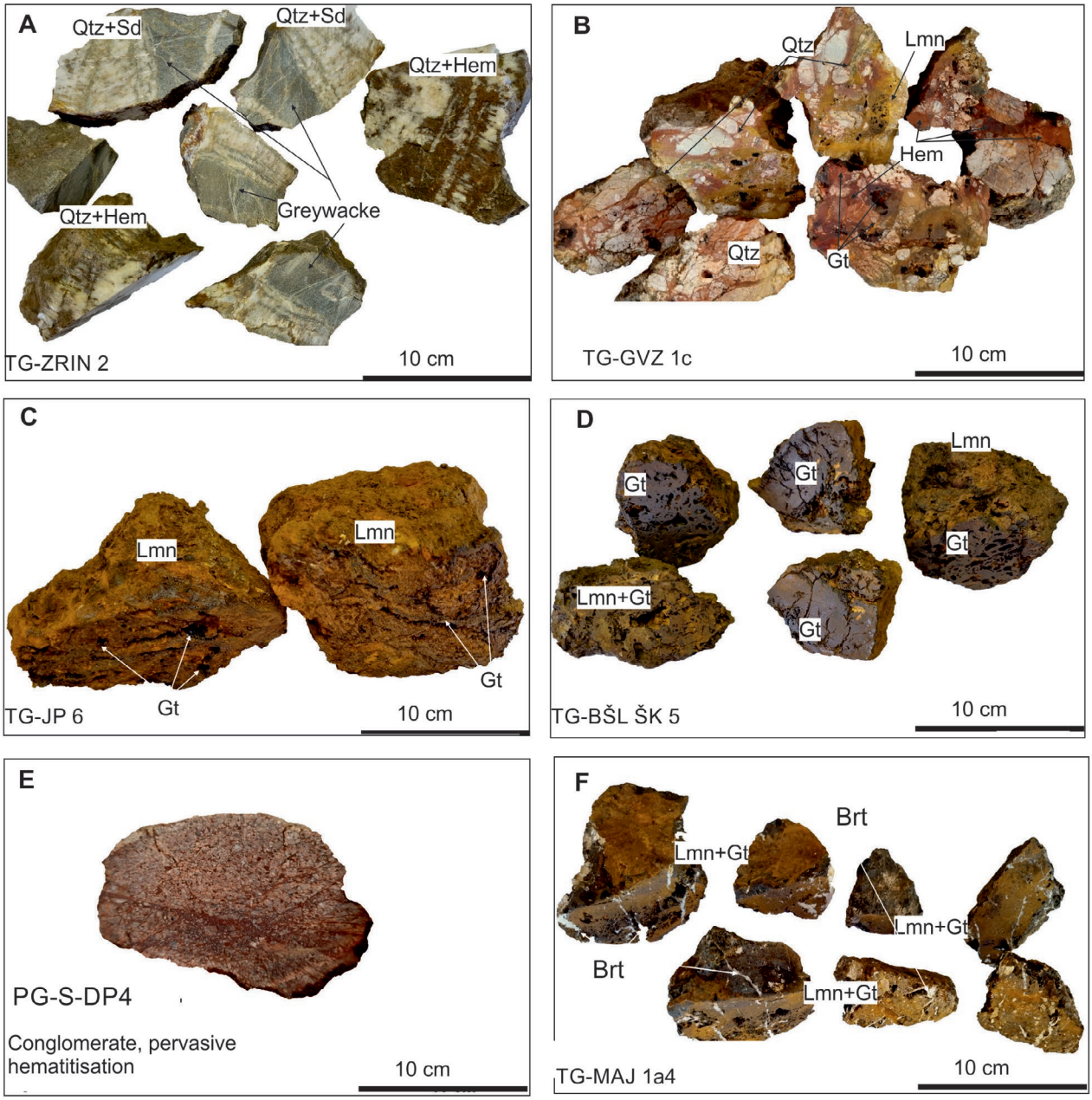

Fig. 3. Samples photographs from TG and PG region. **(A, B)** Primary TG ore localities. A – Zrin locality weakly-moderately altered greywacke cross cut by Qtz–Sid or Qtz–Hem veins; B – Gvozdansko locality, Qtz–Sid–Hem–Gn veins. **(C, D)** TG Proximal secondary ore (gossan). C – Jokin potok locality; D – Školski brijeg locality – heavily weathered iron ore with colloidal goethite. **(E, F)** Primary PG locality. E – Conglomerate with pervasive hematitization of the matrix; F – limonite goethite and minor baryte, cavernous.

Secondary Fe-mineralisation:

At Majdan, forestry works exposed iron ore lenses in soil at 40–70 cm depth (Fig. 2G). These lenses consist of rounded Fe pebbles with varying degrees of weathering (Supplementary Table S1). Micropetrography reveals textures similar to primary mineralisation in quartz greywacke. The host rock is clast-supported, weakly sorted quartz-greywacke with angular quartz and detrital muscovite. The matrix is recrystallised sericite–quartz–siderite–opaque minerals crosscut by veinlets up to 0.25 mm thick.

XRD (Table 2) shows goethite (α-FeO(OH)) and quartz as dominant phases, with illite-sericite and hematite, siderite, calcite, lepidocrocite (γ-FeO(OH)) and todorokite ($(Na,Ca,K,Ba,Sr)_{1-x}(Mn,Mg,Al)_6O_{12}\cdot 3–4H_2O$). Several phyllosilicate phases, including probable occurrences of kaolinite, chlorite and vermiculite, are also detected.

Proximal bog iron ore occurs several metres below Bešlinec–Šestina Kosa and Jokin Potok mine-dumps along stream edges (Supplementary Table S1). Samples show colloidal concentric Fe-oxyhydroxide with quartz, mica and chlorite

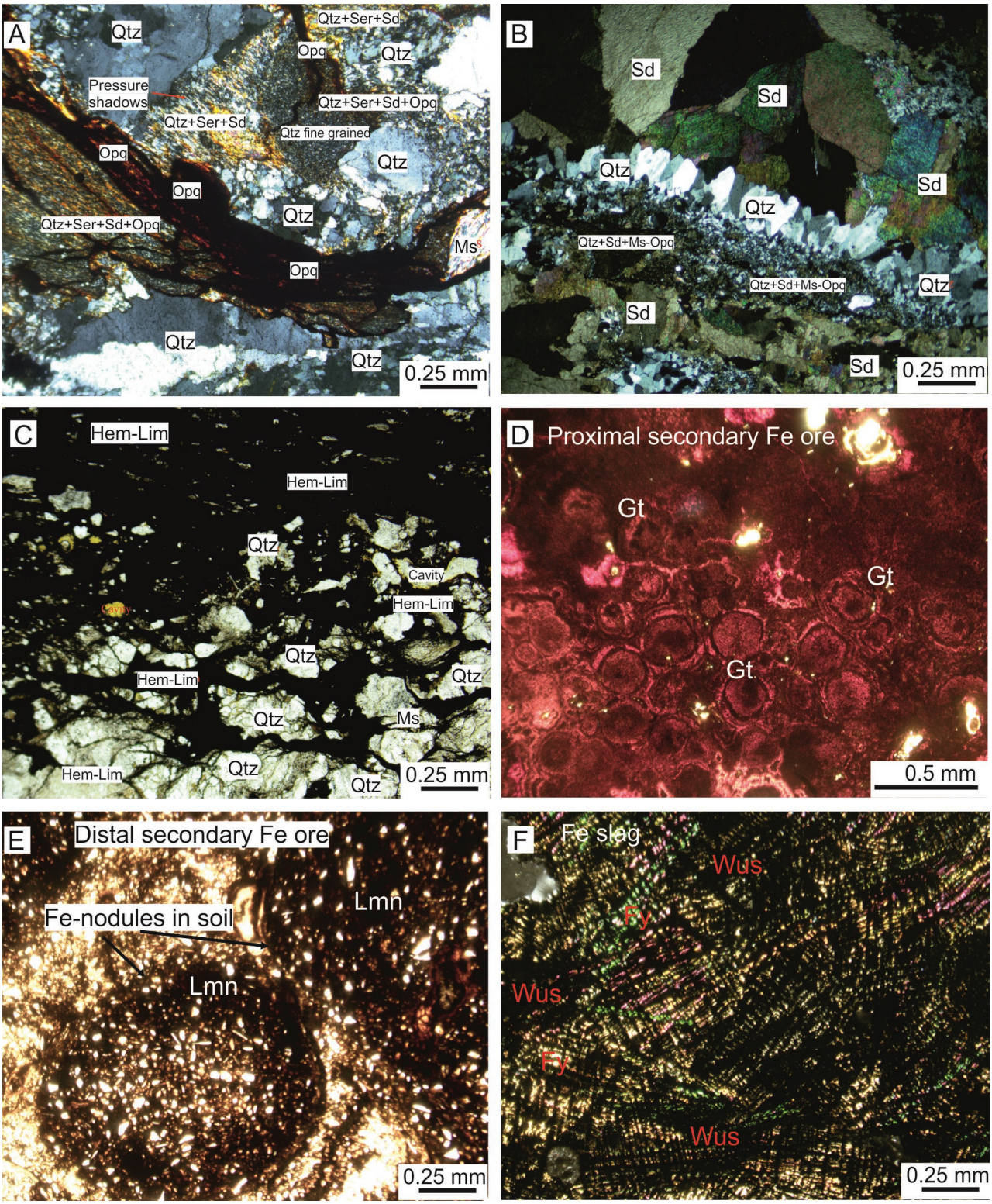

Fig. 4. Selected microphotographs from TG region. **(A–C)** Primary ore: A – Gvozdansko locality, quartz–sericite–siderite–opaque minerals matrix /veinlets within coarse-grained sandstone. Pressure shadows composed of fibrous quartz and/or muscovite and opaque minerals decorate fine-grained quartz clasts. B – Zrin locality. Mineralised veins within greywacke filled with coarse-grained siderite (haematitised), quartz, titanium minerals (titanite–rutile). C – Vidoria locality. Ore breccia composed of quartzite clasts cemented by limonite–hematite. **(D–E)** Secondary ore: D – Bešlinac-Šestina kosa locality. Colloidal concentric forms of Fe-oxyhydroxide with sporadic angular fragments of quartz, mica and chlorite. E – Hrastovica locality Fe-rich soil with nodular, concentric masses of very fine-grained Fe-oxyhydroxide suppressing soil matrix forms encompassing quartz, mica and chlorite, within soil. **(F)** Archaeological slag showing crosshatched (tartan-like) pattern of composite growth of high interference fayalite and opaque wüstite.

Table 2: Semi-quantitative mineral abundances derived from X-ray diffraction data of moderate to heavily altered primary and secondary iron-ore samples from TG (21), PG (8) and lowland (2). Relative abundances are classified as major (+++), minor (++), and trace (+) based on diffraction peak intensities, while ? denotes tentative phase identification due to weak or overlapping peaks.

Location		Sample Name	Qtz	Gt	10Å	7Å	14Å	Chl	Hem	Sd	Other minerals
TRGOVSKA GORA Mt.											
PRIMARY ORE	GVOZDANSKO	TG – GVZ1a	+	++++	+						
		TG – GVZ1b	++	++	+	+	?	?			
		TG – GVZ1c	+++	+	+	+	?	+			Tdr
		TG – GVZ1d	+++	+	+						Rt, Tdr?
		TG – GVZ5	++	+	+	?	?	+		+	Rt, Tdr?
	BEŠLINEC - ŠESTINA KOSA	TG – BŠL-Škosa2b	+++	++	++	+		+		+	Rt; Tdr?
		TG – BŠL-Škosa6a	+	++++	+				+		
		TG – BŠL-Škosa6b	++	++	+	?	?	?	+		
	ZRIN	TG – ZRIN1	++	++	+	?	?	+	+	+	Sp, Gn
	JOKIN POTOK	TG – JP1a	+++	++	++	+	?	?			
		TG – JP3	+	++++	+	?	?	?	+		
		TG – JP5	+	+++	+	?	?	+			
		TG – JP6	+	+++	?	+	?	?	+		
	VIDORIJA	TG – VID2a		+++					+++		
		TG – VID2b	+++	+++	+	?	+	+			Rt
		TG – VID3	+++	++	+						
SECONDARY ORE	MAJDAN	TG – MAJ1a2	+++	++	++	+	?	+			Cal, Lpc
		TG – MAJ1a3	++	++	+	+	?	+	+		Cal
		TG – MAJ1a4	++	++	+	+	+	+		?	Cal?, Tdr?
	BEŠLINEC - ŠESTINA KOSA	TG – BŠL-Škosa5	+	++++	+						
		TG – BŠL-Škosa2a	+	++++	?		?	?	+		Py
	JOKIN POTOK	TG – JP6	+	+++	?	+	?	?	+		
SLAG		TG – JP4									Fy, Wus
PETROVA GORA Mt.											
PRIMARY ORE	PECKA	PG – PEC1	+	++++	+	?	?	?			
		PG – PEC3a	+++	+/++	+	?	?	+			
		PG – PEC3b	++	++	+	?	?	+			
		PG – PEC4b	++	+++	+	?	?	?			
		PG – PEC5	++	+++	+	?	?	+			
	KIJAK (SAMOGRAD-DUBOKI POTOK)	PG – S-DP- 1a	+	+++	?						Brt
		PG – S-DP- 1b	++	++	+	?					Brt
		PG – S-DP-3	?	+++	?	?					Brt
LOWLAND BETWEEN TRGOVSKA AND PETROVA GORA Mts.											
DISTAL SECONDARY ORE	OSEKOVO	OS-1	+++	? / +	++	?	+	+			
	HRASTOVICA	HRAS-3	+++	+	++	+	+	+			Cal, Dol

fragments (Fig. 4D), with older bog iron fragments sporadically incorporated. Additionally, sample from Bešlinec–Šestina Kosa contains an autogenic pale green-blue radial mineral (Table 2). XRD shows goethite as dominant mineral phase, with subordinate quartz, pyrite and hematite. Mica mineral phases (10 Å), as well as 7 and 14 Å phyllosilicates, such as kaolinite, chlorite and vermiculite, are probably present, based on noticeable doublet peaks at 14.27, 14 as well as 7.14 and 7 Å peaks.

Archaeological slag:

Tap iron slag from Jokin Potok consists of dendritic networks of Fe-rich olivine (fayalite) and opaque minerals. XRD shows fayalite and wüstite as the main phases, typical for direct-reduction slag (Fig. 4F).

Petrova Gora

Host rocks and primary hydrothermal Fe (Ba) mineralisation:

Mineralisation at Petrova Gora closely resembles that at Trgovska Gora. Iron-bearing veins and veinlets are found in fine- to coarse-grained sandstone, greywacke, and conglomerate rocks (Fig. 3E,F). Coarse-grained baryte–goethite (limonite) veins and breccias are also present.

The matrix-supported, poorly sorted greywacke consists mainly of angular to subrounded quartzite clasts up to 0.50× 0.9 mm in size, which are heavily fractured and recrystallised, along with fine-grained quartz clasts and elongated detrital mica (up to 0.1×0.45 mm). The fine-grained matrix of sericite

and opaque minerals is crosscut by opaque–sericite veinlets (Fig. 5A, B).

Matrix-supported conglomerate contains rounded polycrystalline quartzite fragments up to 6×8 mm, partly recrystallised and typically grading from larger undulose subgrains to smaller ones. Silicified clasts and typical greywacke sandstone clasts are also present. Clasts are either embedded within a fine- to medium-grained quartz–sericite–opaque matrix showing regular limonitisation (Fig. 5C) or cut by <1 mm weakly parallel veinlets of limonitised opaque minerals containing disintegrated detrital quartz fragments.

Ore breccia consists of fragments of matrix-supported, poorly sorted greywacke with angular to subrounded quartzite clasts (up to 0.20×0.5 mm) and detrital mica (up to 0.1×0.75 mm) in a fine sericite–opaque matrix, and polycrystalline coarse-grained quartzite (non-undulose to weakly undulose) with muscovite crosscut by opaque veinlets. Baryte occurs as coarse grains (>1 cm) cemented by fine-grained baryte (0.1×0.2 mm; Fig. 5D).

Heavily altered samples from Petrova Gora containing >50 wt% limonite/goethite were analysed by X-ray diffraction (Table 2). Results show major minerals similar to those at Trgovska Gora: goethite as the predominant phase, followed by quartz and a 10 Å mineral, likely illite–sericite. The minor mineral assemblage is modest. In samples from the Kijak location, baryte sometimes exceeds quartz in abundance, while albite occurs in samples from Pecka.

Mineralisation within lowland between Petrova and Trgovska gora Mts.

Several samples of limonite–goethite, including nodular concretions and irregular fragments (0.2–5 cm) were collected from the topmost part of ploughed soils (up to 25–30 cm

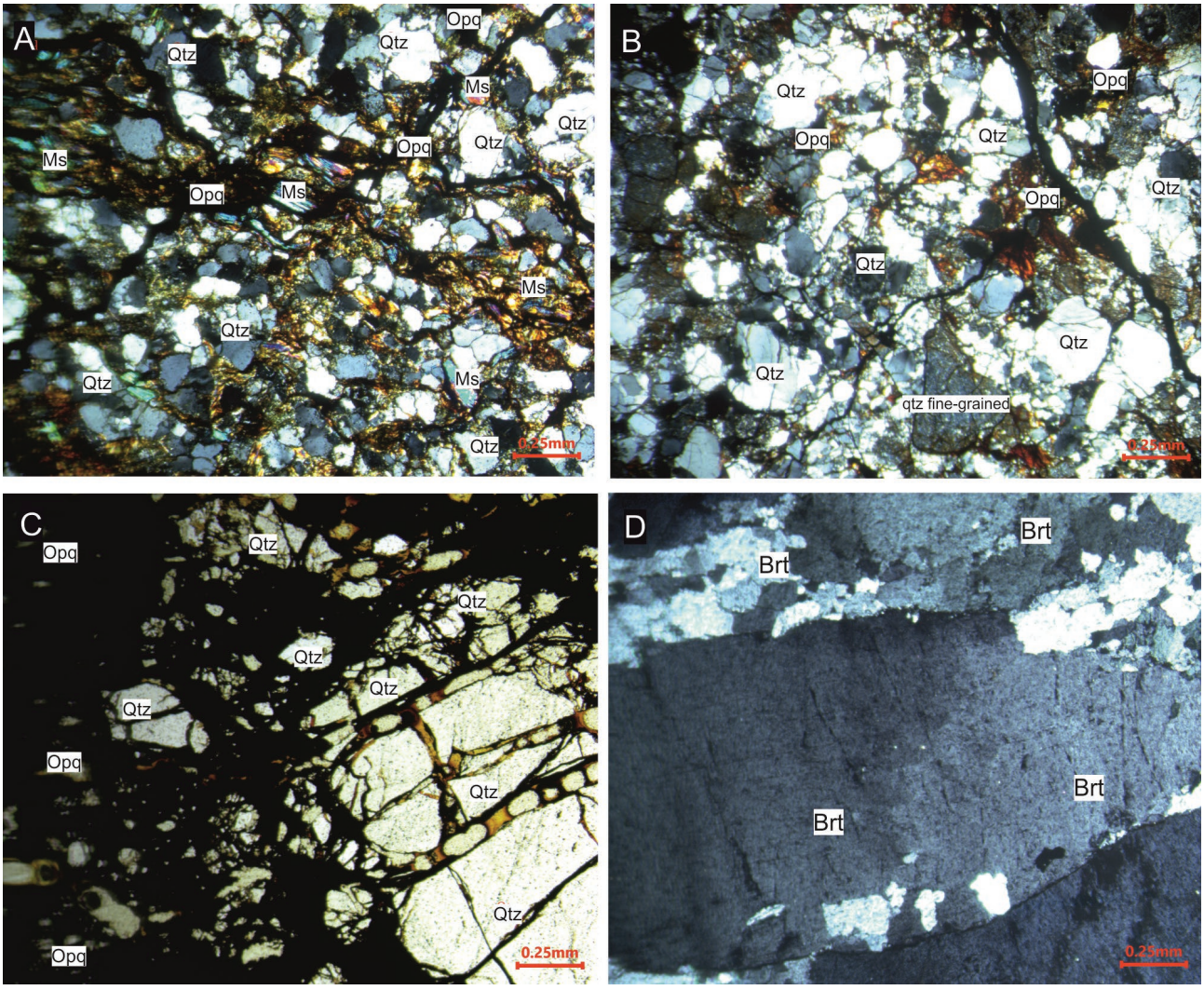

Fig. 5. Selected microphotographs from PG region. **(A, B)** Pecka locality. Weakly sorted greywacke composed of angular to subrounded quartzite and quartz clasts in fine-grained matrix of sericite and opaque minerals, crosscut by opaque–sericite veinlets. **(C, D)** Samograd–Duboki potok locality. C – Mineralised conglomerate; D – Monomineralised baryte vein.

depth), and along the stream banks in the lowland between the Petrova and Trgovska gora regions (Fig. 6A). Micropetrography reveals Fe-rich soil containing nodular forms composed of angular fragments of quartz (up to 0.06×0.07 mm in size), mica and chlorite (up to 0.1×0.01 mm in size), embedded within concentric masses of very fine-grained Fe-oxyhydroxide, which suppresses the soil matrix (Fig. 6B,C). X-ray diffraction shows predominant quartz, followed by subordinate illite-smectite, goethite, 7 Å and 14 Å clay minerals and chlorite. Additionally, the sample from Hrastovica shows a predominance of carbonate minerals (calcite and dolomite).

Geochemistry

Principal Component Analysis (PCA) and Hierarchical Cluster Analysis (HCA) were used to investigate geochemical relationships and sample groupings on the bulk geochemical data set. Thirty-five elements and the summed rare earth element (ΣREE) concentrations were included as variables, with the first three principal components (PC1–PC3) explaining 60 % of the total variance (Fig. 7A; Supplementary Table S4). Although PCA does not quantify correlations, the relative orientation and sign of variable loadings allow recognition of association patterns. In the PCA loading space, Fe_2O_3 groups with Ba, and Sr, and show inverse relationship with the Al_2O_3–SiO_2–Na_2O–K_2O–TiO_2–ΣREE cluster, together with immobile elements such as Zr, Hf, Ta, Cr. Base metals (Cu, Pb, Zn, Ag, Co, Ni, Sn, Cd, Sb, As) and sulphur form a separate group. These loading patterns reflect multiple geochemical controls related to: (i) alumosilicate host rocks; (ii) early hydrothermal stage responsible for siderite mineralisation, and (iii) later hydrothermal stage responsible for base metals sulphide assemblages (sensu Borojević Šoštarić et al. 2009).

Sample distribution along the principal components highlights systematic differences between ore and deposit types. Primary and proximal secondary mineralisation from both Petrova Gora (PG) and Trgovska Gora (TG) cluster together along PC1 without clear separation, whereas secondary distal ores from lowland areas are more distinctly differentiated. Outliers plotting in the positive PC2 space correspond to primary or proximal secondary ores with pronounced sulphide mineralisation (TG-ZRIN1 and TG-GVZ5) and to samples enriched in base metals (TG-MAJ1a2), indicating zones of polymetallic Fe–Cu–Pb mineralisation.

The HCA results (Fig. 7B; Supplementary Table S4) further support the PCA findings. Five minor clusters were defined at the first major step in the dendrogram where a marked increase in linkage distance occurs (cut-off linkage distance=11.3), reflecting distal incipient bog iron ores from the lowland areas of the Sava River and its tributaries, primary and secondary polymetallic Fe–Cu–Pb deposits from the TG Mountains, primary monometallic Ba-enriched deposits from the PG Mountains, Mn-enriched monometallic Fe deposits from the TG Mountains, and primary and secondary monometallic deposits from both TG and PG. The analysis also reveals a tendency for samples to cluster according to their specific locality, reflecting the proximity of deposits regardless of the ore type (primary or secondary proximal). This pattern is particularly evident for some TG samples, which form a separate cluster. The slag sample (TG-JP4) groups with the primary and secondary ores from the location where it was collected, further supporting the locality-driven clustering pattern.

Both statistical methods demonstrate that bulk geochemical analysis of samples found within the same region, can differentiate between different types of deposits. However, substantial similarities persist between primary and proximal secondary iron ores from monometallic Fe deposits in both areas, the TG and PG Mts., testifying to a strong, correlating hydrothermal signature.

To further characterise intra-regional differences by area and ore type, detailed geochemical analyses is undertaken for each of these categories.

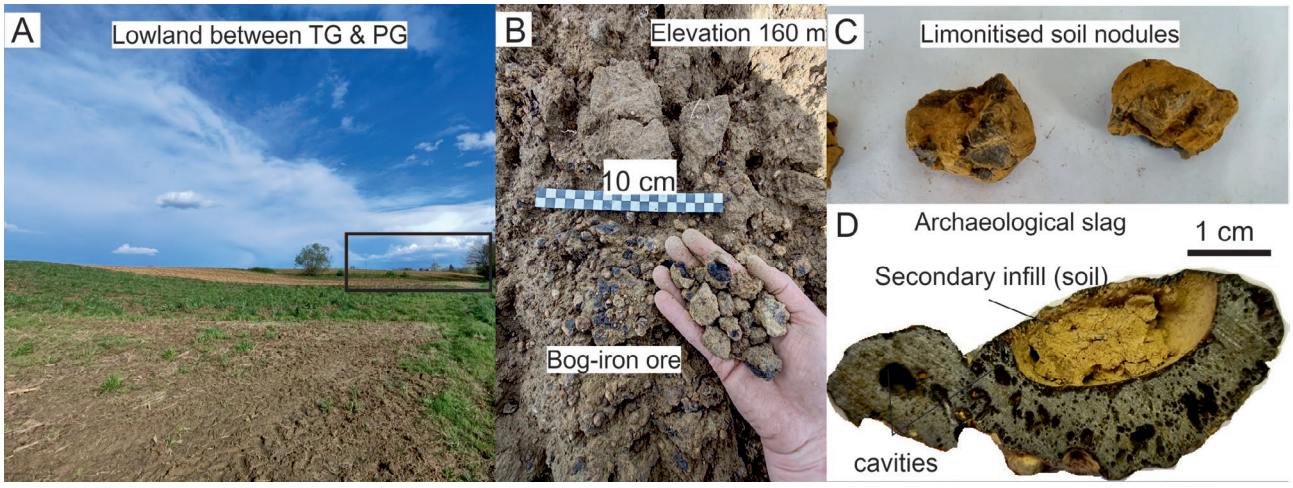

Fig. 6. Sample photographs from lowland – secondary ore. **(A, B)** Osekovo filed photography, black frame pointing to sampling location of Fe oxyhydroxide nodule from topmost soil at 160 m a.s.l. **(C)** Buzeta limonitised soil nodules. **(D)** Archaeological slag.

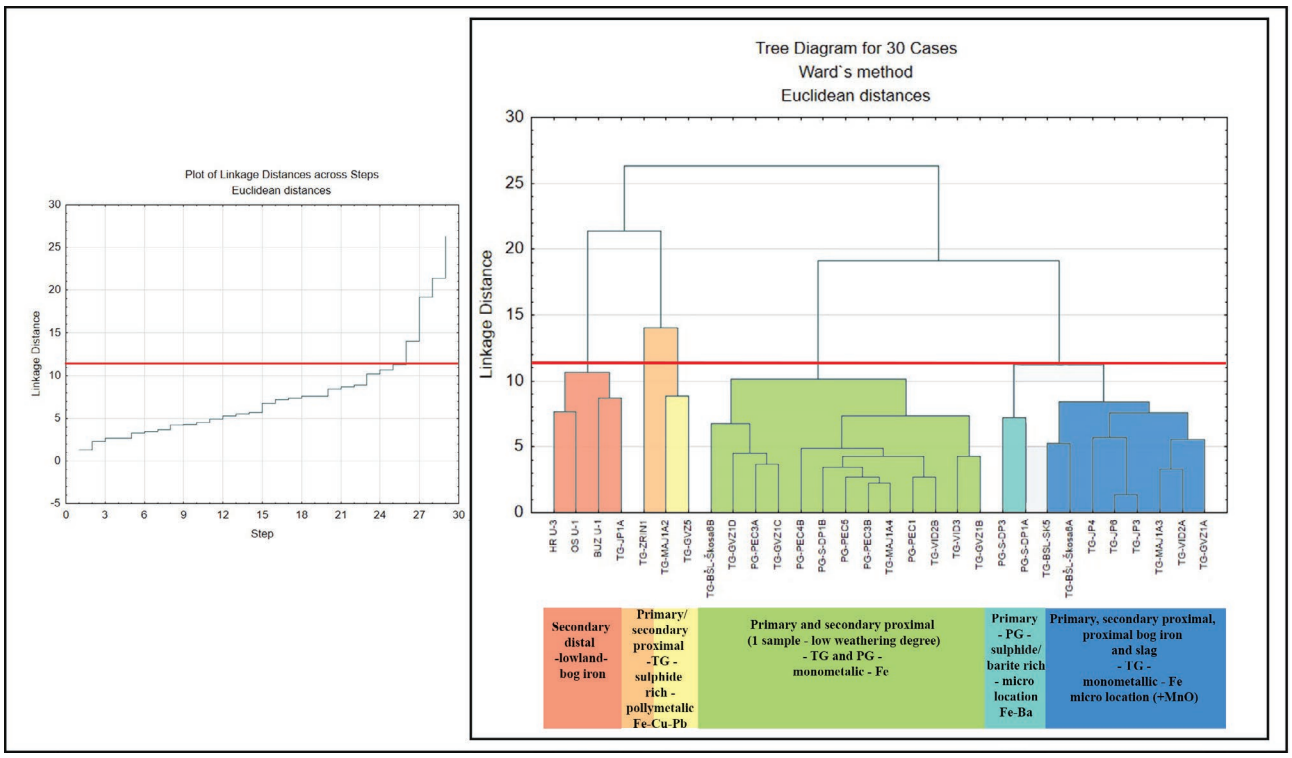

Fig. 7. (A) PCA loading space of based on bulk geochemistry of all samples. **(B)** Hierarchical clustering diagram based on bulk geochemistry of all samples. See text for discussion.

Trgovska Gora

Host rocks and primary hydrothermal Fe (Cu, Pb) mineralisation:

Thirteen TG samples of mineralised sandstones, conglomerates and ore breccias show highly variable composition. Fe_2O_3 ranges from 8.8 to 86 wt%, SiO_2 from 2.2 to 79.6 wt% and Al_2O_3 between 0.2 and 8.4 wt%, with generally high LOI (2.1–24.9 wt%). CaO, MgO and Na_2O are mostly below 1 %, except for one Gvozdansko sample (4.8 wt% MgO). MnO reaches 6.2 wt% at Jokin Potok, Majdan and sporadically at Vidorija and Bešlinec, but is lower at Gvozdansko.

Fe_2O_3 is negatively correlated with hydrothermal base metals, SiO_2, Al_2O_3, K_2O and Na_2O, and positively with MnO and P_2O_5, indicating three sample types; aluminosilicate host rocks, siderite and base-metal phase of mineralisation (Supplementary Tables S2, S3). This is consistent with observation of Borojević Šoštarić et al. (2009), reporting two-stage formation of Fe-bearing mineralisation, initial siderite phase precipitated at slightly higher temperature was followed by later stage quartz–polysulphide phase. SiO_2–Al_2O_3–K_2O–Na_2O correlate with Mo, V and Th, while Fe_2O_3 shows a weak positive correlation with U. Hydrothermal base metals and sulphur are enriched (ΣCu, Pb, Zn, Ag, Co, Ni, Sn, Cd, Sb, As, SO_3, Ba, Sr>3 wt%), especially at Gvozdansko and Zrin (SO_3 up to 0.8 wt%, Pb>1 wt%, Zn>1 wt%).

LILE and HFSE mostly plot between 0.01 and 1, with positive Ba, U and P anomalies and a strong negative Sr anomaly (Fig. 8A). REE patterns are concave, with low light REE, slightly enriched mid-REE and flat heavy REE (Fig. 8B). Several Fe-rich (>75 wt% Fe_2O_3) samples show negative Ce and strong positive Eu anomalies, consistent with REE adsorption onto Fe(III)-oxyhydroxides during weathering (Tyler 2004; Ramos et al. 2016). These heavily weathered samples cluster with secondary Fe mineralisation in the HCA (Supplementary Table S3).

Secondary Fe mineralisation:

Five proximal secondary ore samples show similar chemistry to primary mineralisation (Fig. 8C, D). Fe_2O_3 ranges from 27.1 to 78.3 wt%, SiO_2 between 4.8 and 50.5 wt% and Al_2O_3 from 1.9 to 10.0 wt%, with LOI ranging from 6.6 to 12.9 wt%. One sample from Bešlinac–Šestina Kosa stands out, containing 2.3 wt% P_2O_5 while MnO peaks at 2.9 wt% at Majdan (Supplementary Tables S2, S3). As with primary ores, Fe_2O_3 correlates negatively with SiO_2–Al_2O_3–K_2O and positively with P_2O_5, while SiO_2 positively correlates with Ba and base metals, while Fe_2O_3 correlates with Mo and U.

Sulphur is low but correlates positively with Cu, Pb, Zn, Sn, Cd, Sb and As. Base-metal totals are lower than in primary ores (<1.6 wt%), but some soil-profile samples show elevated Cu, Pb, Zn, Sb and As. LILE–HFSE patterns and REE distributions resemble primary mineralisation, with negative Ce and positive Eu anomalies (Fig. 8C, D).

Archaeological slag:

A single slag sample from Jokin Potok contains 71.8 wt% Fe_2O_3, 21.8 wt% SiO_2, 4.6 wt% Al_2O_3 and 4.9 wt% MnO,

comparable to nearby Fe ores (Figs. 1, 6D; Supplementary Tables S2, S3). Ba enrichment mirrors secondary ores. Negative LOI (−5.1) reflects high-temperature smelting (1100–1300 °C). LILE–HFSE and REE patterns closely match proximal secondary ores, with negative Ce and pronounced positive Eu anomalies (Fig. 8C, D).

Petrova Gora

Host rock and primary hydrothermal Fe (Ba) mineralisation:

Eight PG sandstone and conglomerate samples exhibit less compositional variation than TG samples. Fe_2O_3 ranges from 23.1 to 76.7 wt%, SiO_2 from 3.9 to 64.2 wt%, and Al_2O_3 from 0.2 to 7.9 wt%, with LOI between 4.7 and 10.7 wt%. CaO, MgO and Na_2O are each below 0.1 %, P_2O_5 peaks at 0.6 wt%. Total MnO values are lower compared to TG region (from <0,1 up to 2.1 wt%). Similarly, total amount of K_2O is also low (up to 1.8 wt%).

Fe_2O_3 correlates negatively with SiO_2, Al_2O_3, K_2O and Na_2O, and positively with SO_3 (Supplementary Tables S2, S3). SiO_2, Al_2O_3, K_2O and Na_2O correlate positively with Pb, As, V, U and Th, as well as with Cu, Zn, Co and Ni, whereas Fe_2O_3 correlates positively with Ag, Cd and Ba. Hydrothermal metal and sulphur contents differ markedly between localities: Pecka samples contain ≤0.2 wt% of the total base metals and SO_3 (Zn, Co, Ni enriched), whereas baryte-rich Samograd–Duboki Potok samples reach 6.6 wt%. Sulphur correlates negatively with Cu, Pb, Zn, Sn, Cd, Sb and As, but positively with Ba, suggesting sulphur occurs largely in baryte.

LILE and HFSE mostly plot between 0.001 and 1, with strong positive Ba and P anomalies and a pronounced negative Sr anomaly (Fig. 9A); U and Sm also show positive anomalies. Microelements increase with Al_2O_3 and decrease with Fe_2O_3, except in baryte-rich samples, which are microelement-poor.

REE patterns differ between localities. Pecka samples show flat profiles with a minor positive Ce anomaly (Fig. 9B), whereas Samograd–Duboki Potok samples are LREE-depleted, MREE-flat and HREE-enriched, with negative Ce and positive Eu and Yb anomalies, indicating weathering under oxidising conditions (sensu Zhang & Shields 2022).

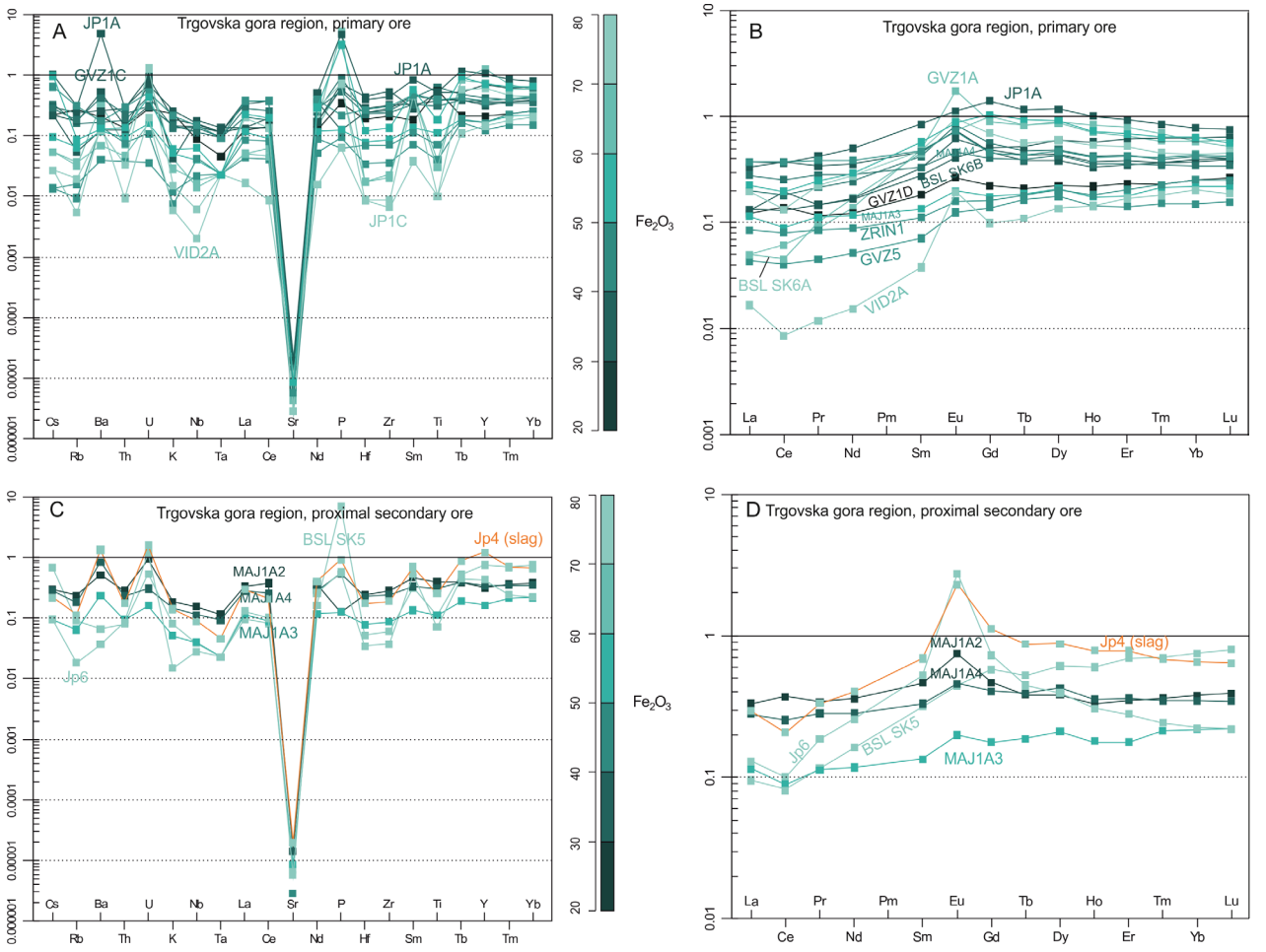

Fig. 8. Geochemical plots for TG ore normalised after Upper continental crust (Taylor & McLennan 1995). **(A, B)** Multi-element and rare-earth element plots for primary TG ore. **(C, D)** Multi-element and rare-earth element plots for secondary TG ore. Samples are correlated with their amount of Fe_2O_3; data taken from Supplementary Table S2. See text for discussion.

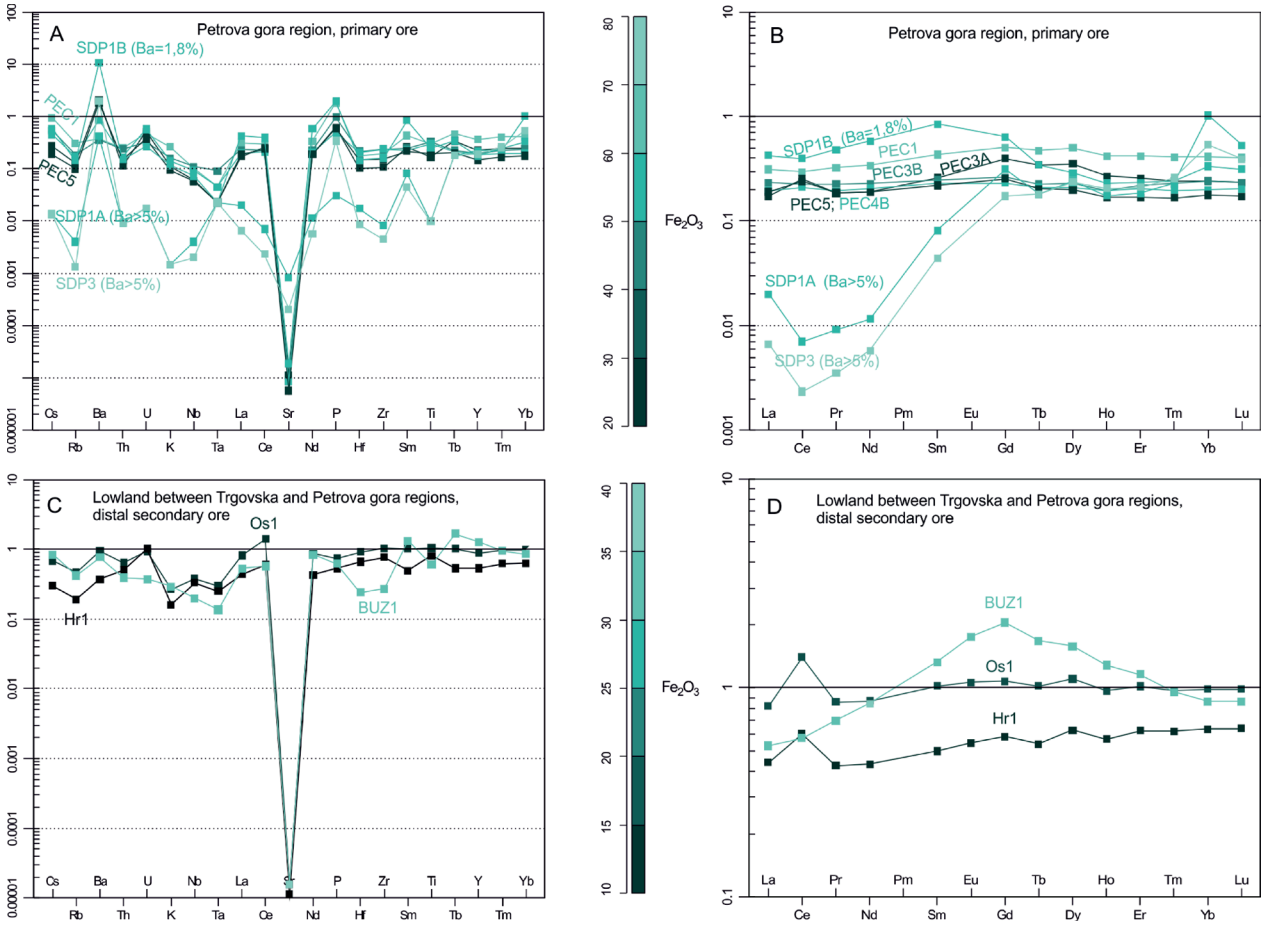

Fig. 9. Geochemical plots for PG primary and lowland ore normalised after Upper continental crust (Taylor & McLennan 1995). **(A, B)** Multi-element and rare-earth element plots for primary PG ore. **(C, D)** Multi-element and rare-earth element plots for secondary lowland ore. Samples are correlated with their amount of Fe_2O_3; data taken from Supplementary Table S2. See text for discussion.

Mineralisation within lowland between Petrova and Trgovska gora Mts.

Three samples of incipient bog iron ore concretions and nodules from the lowland between the Trgovska and Petrova Gora regions show variable increased total iron contents (9.6–34.7 wt% Fe_2O_3) comparing too upper continental crust (Rudnick & Gao 2003), however significantly lower than observed in primary and proximal secondary ore, and high SiO_2 (35.7–58.5 wt%) and Al_2O_3 (12.4–14.1 wt%). LOI values range from 6.8 to 17.4 wt%, CaO is up to 10.2 wt%, MgO up to 4.1 wt%, and MnO up to 1.6 wt%. Total P_2O_5 and Na_2O are below 1 wt%. There is a positive correlation between SiO_2, Al_2O_3, Na_2O and P_2O_5, Pb, Co, As (Supplementary Table S3). Fe_2O_3 correlates positively with aluminosilicates, P_2O_5, Cu, Zn, Cd, V, and Ba, whereas Mo correlates positively with SO_3. These total contents of major oxides and correlation trends differ from the primary and secondary mineralisation in the PG and TG regions, explaining the clear segregation of samples into a specific cluster in HCA and their separation in the PCA plot (Supplementary Tables S2, S3). The sum of hydrothermal base metals and sulphur is much lower compared to the PG and TG regions, ranging between 540 and 980 ppm. Hydrothermal base metals generally correlate with each other.

General trends on multi-element plots are similar to those in the TG and PG regions, with the majority of microelements between 0.1 and 1, a positive Ba and U anomaly, and a pronounced negative Sr anomaly (Fig. 9C). Again, general enrichment of microelements follows Al_2O_3, while a general decrease of microelements follows Fe_2O_3. The REE trend shows a slightly concave shape, with slightly enriched MREE compared to LREE and HREE, and weak positive Eu and Ce anomalies in two samples (Fig. 9D).

Discussion

The regional geochemical signature

The geochemical character of the TG and PG mountains reflects their host rock composition, primary mineralisation, and secondary weathering. Six key features define the regional signature (Fig. 10):

(1) High iron content

Iron is the most prominent feature in both TG and PG, clearly recording both primary mineralisation and secondary enrichment. TG samples reach up to 86 wt% Fe_2O_3, with values typically between 30 and 75 wt% (Fig. 10A). Secondary ores are strongly enriched, with a median of ~65 wt% Fe_2O_3 compared to ~45 wt% in primary ores, reflecting oxidation-driven enrichment. PG ores show a narrower and slightly lower Fe_2O_3 range compared with TG, while distal lowland ores are much poorer (median ~15 wt%).

The distal samples are likely not representative of fully mature deposits. Field textures (hardened nodules) and published comparisons suggest they represent an early developmental stage of bog iron formation, linked to initial groundwater Fe precipitation (Thelemann et al. 2017; Brenko

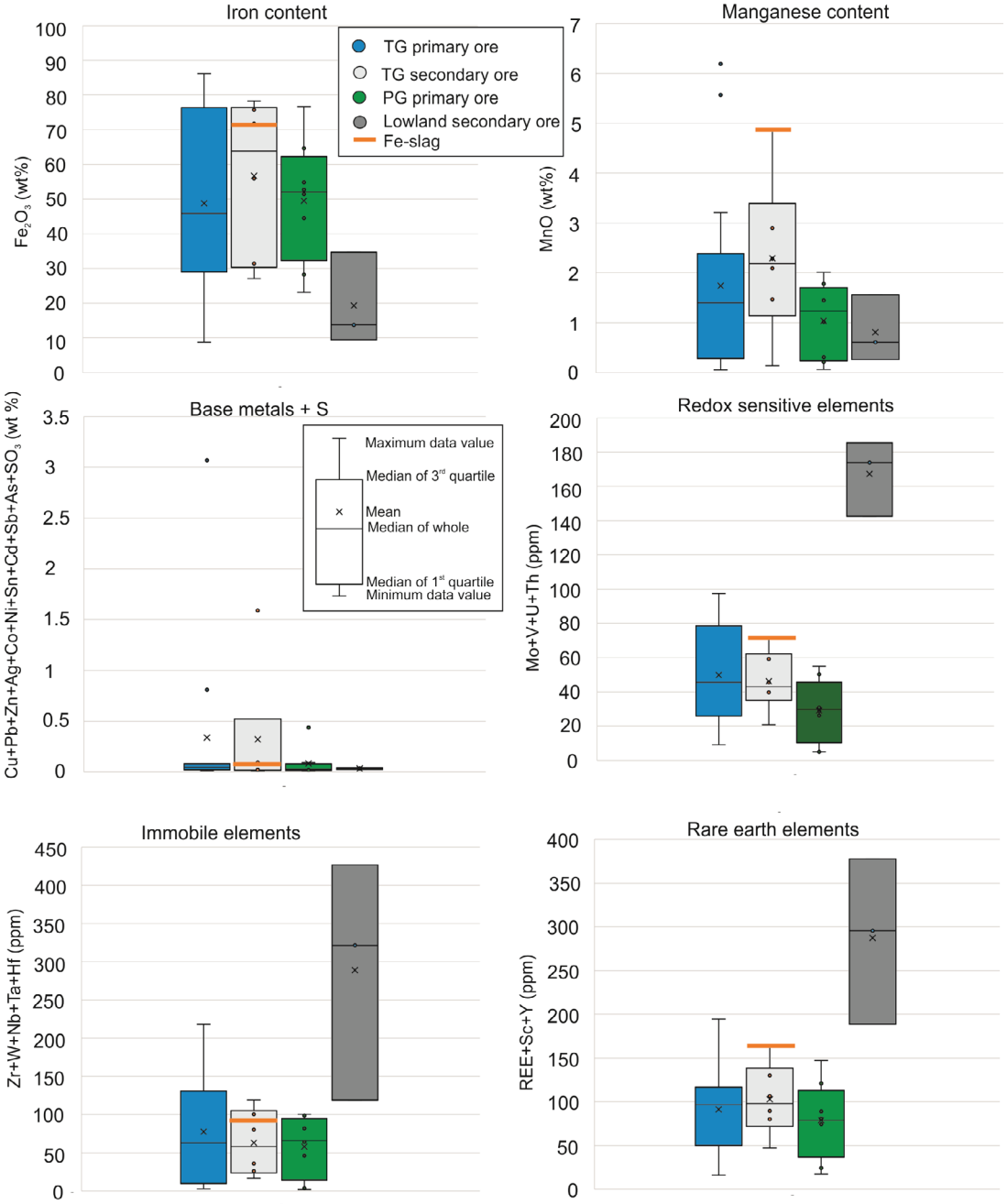

Fig. 10. Statistical analysis of selected sets of elements for TG primary and secondary, PG primary and lowland secondary ore showing maximum and minimum, mean, median and middle 50 % of the values. Position of Fe-slag is given in orange. **(A–C)** Hydrothermal mineralisation signature: A – Fe_2O_3 in wt%; B – MnO in wt%; C – Sum of hydrothermal metals, sulphur and barium (Cu+Pb+Zn+Ag+Co+Ni+Sn+Cd+Sb+As+SO_3) in wt%. **(D–F)** Host flysch rocks signature: D – Sum of redox sensitive elements (Mo, V, U) in ppm; E – Sum of immobile elements (Zr, W, Nb, Ta, Hf) in ppm; F – Sum of rare earth elements (REE+Sc+Y) in ppm. Data taken from Supplementary Table S2. See text for discussion.

et al. 2021; Karavidović & Brenko 2022). With further development, nodules agglomerate or undergo intense Fe cementation, suppressing the aluminosilicate matrix and raising total Fe contents, as seen in bog iron from the Drava River plain in NE Croatia (68–70 wt% Fe_2O_3; Brenko et al. 2020, 2021).

Mineralogical observations support these trends. Siderite, goethite, hematite, lepidocrocite, and amorphous Fe phases occur in matrix and veinlets, either preserved or transformed during weathering. The negative Fe–S and Fe–base metal correlations in TG suggest a siderite → quartz–sulphide → baryte sequence, while PG shows positive Fe–Ba–SO_3 and negative Fe–base metal relationships, consistent with siderite–baryte followed by quartz–sulphide mineralisation (Borojević Šoštarić et al. 2009).

(2) High manganese content

Manganese is another diagnostic geochemical marker, locally reaching 5–6 wt% MnO at Jokin potok and Bešlinec–Šestina kosa, where black amorphous Mn oxyhydroxide precipitates were observed in streams draining collapsed mine adits (Fig. 2D). Mineralogical data confirm this enrichment: todorokite was identified by XRD in samples from Gvozdansko and Majdan, while psilomelane was recognised in earlier studies (Jurković 1959). This is consistent with observation from nearby Ljubija siderite deposit, where Strmić Palinkaš et al (2009) reported increased manganese values in siderite mineralization, especially high for so called *zebra* siderite (up to 3.2 wt% of MnO).

Geochemically, secondary ores are clearly enriched in Mn (median >2 wt% MnO), compared to <1.5 wt% in primary TG and PG ores (Fig. 10B). Within TG, primary ores are slightly richer than PG, which shows a low median (0.5 wt% MnO). Distal lowland ores overlap with PG values, suggesting that significant Mn enrichment is limited to proximal secondary environments.

(3) High base-metal contents

Base metals are a key feature of TG and PG mineralisation, though with contrasting parageneses. TG hosts a complex polysulphide assemblage including pyrite, chalcopyrite, galena, arsenopyrite, Ni–Co gersdorffite, Ni-linnaeite, millerite, sphalerite, Ag-tetrahedrite, tennantite, cassiterite, enargite, bournonite, boulangerite, chalcocite, covellite, millerite, bravoite, and Ag-minerals (Jurković 1959, 1962, 1988; Jurković & Durn 1988; Borojević Šoštarić et al. 2009). In contrast, PG displays a simpler sulphide paragenesis dominated by pyrite, chalcopyrite, sphalerite, and tetrahedrite, with baryte as the predominant associated mineral (Borojević Šoštarić et al. 2009).

Based on these assemblages, hydrothermal origins are inferred for Cu, Pb, Zn, Ag, Co, Ni, Sn, Sb, and As, as well as Ba (in PG) and S. Geochemical data support these mineralogical observations: the middle 50 % of values for primary TG and PG ores are below 0.1 wt%, whereas TG secondary ores commonly exceed 0.5 wt% (Fig. 10C). Numerous outliers (>0.25 wt%) occur in both primary and secondary ores, with cumulative base metal contents sometimes reaching several wt%.

Correlation patterns reflect these differences. In TG, base metals in both primary and secondary ores correlate strongly and positively with sulphur (and with one another), consistent with abundant sulphide mineralisation. Chalcopyrite, galena, pyrite, and sphalerite (Table 2) were directly observed in TG samples. In PG, however, primary ores contain no identifiable sulphides, and base metals correlate negatively with sulphur. This pattern is attributed to extensive weathering of sulphide precursors.

The absolute abundance of base metals is also lower in PG compared to TG. Here, Cu, Zn, Co, Ni, As, and Pb correlate positively with the aluminosilicate fraction (illite, smectite, chlorite; Table 2). Metals may be present as nanoscale inclusions, adsorbed ions on clay surfaces, or as structural substitutions within phyllosilicates (Klein 2003 and references therein). Laboratory evidence supports this process: Orucoglu et al. (2022) demonstrated that Pb^{2+} and Co^{2+} at low pH are readily adsorbed via cation exchange at basal surfaces between two TOT layers (tetrahedral–octahedral–tetrahedral).

Baryte is a further distinctive feature in PG. Positive S–Ba correlations and strong Ba–Sr correlations (Supplementary Table S3) reflect baryte crystallisation with partial Sr^{2+} substitution. Although baryte and celestite can form isostructural solid solutions, their contrasting cation radii and solubilities (Ba=1.61 Å; Sr=1.44 Å; Ksp baryte=$10^{-9.97}$; celestite=$10^{-6.63}$ at 25 °C) mean natural compositions are typically close to the end-members (Jacobsen et al. 1998; Weber et al. 2016 and references therein). Elevated Sr in baryte has also been described from the Žune Ba–F deposit in Bosnia and Herzegovina, hosted in the TG flysch (Borojević Šoštarić et al. 2022), as well as hydrothermal baryte in other parts of the Dinarides (Palinkaš & Jurković 1994; Jurković et al. 2010) and the Alps (Barbieri et al. 1982).

Finally, distal lowland ores show lower absolute base metal contents, with a middle 50 % around 0.06 wt%. Nevertheless, they are still at least ten times enriched compared to the upper continental crust (44 ppm; Rudnick & Gao 2003).

(4) Redox sensitive elements (Mo, V, U)

Redox-sensitive elements, particularly U, V, and Mo, are strongly enriched compared to the upper continental crust, with their sum in UCC at 4.1 ppm (Rudnick & Gao 2003), where their concentrations are typically very low (Tribovillard et al. 2006; Bennett & Canfield 2020). In TG ores, both primary and secondary, median values are approximately 45 ppm, with the middle 50 % of data between 25 and 80 ppm. PG ores are slightly lower, with a median of about 30 ppm.

Despite field evidence of ongoing mine drainage and associated redox fluctuations in the region (Fig. 2B–D), these

elements appear relatively immobile during weathering. Statistical correlations link Mo, V, and U with the aluminosilicate fraction (illite, smectite, chlorite), particularly in PG samples (Supplementary Table S3). This is likely due to the preferential adsorption of molybdenum onto clay minerals at low pH (~3; Goldberg et al. 1996), particularly kaolinite and illite, which are abundant in the studied samples. In the case of vanadium, Pan & Fleet (1992) describe the principal octahedral substitution between Al^{3+} and V^{3+} in primary silicates, with V^{3+} remaining concentrated in associated clay minerals during weathering. A notable exception is uranium in TG ores, which shows a weak positive correlation with Fe_2O_3 and MnO in primary samples, increasing to a strong correlation in secondary ores, suggesting uranium may be redistributed during oxidation. In oxidative weathering environments, uranium occurs predominantly as U(VI) in the form of the uranyl ion (UO_2^{2+}), which strongly adsorbs onto iron and manganese oxyhydroxides that are widespread at TG region. This process is particularly significant under low-pH conditions (Sherman et al. 2008).

Distal lowland ores show exceptional enrichment, with a median of approximately 175 ppm (n=3). Although the dataset is small, this pattern indicates enhanced concentration of redox-sensitive elements during transport and secondary accumulation.

(5) Immobile elements (Zr, W, Nb, Ta, Hf)

High field strength elements (HFSE: Zr, W, Nb, Ta, Hf) are generally immobile during chemical weathering, making their distribution a useful tracer. Their total abundance in the UCC is approximately 225 ppm (Rudnick & Gao 2003). In TG and PG ores, including secondary samples, values are consistently depleted, with medians of 55–60 ppm and the middle 50 % ranging between 10 and 130 ppm. In contrast, distal lowland ores are significantly enriched, with a median of approximately 320 ppm.

Multielement plots normalised to the UCC show that HFSE positively correlate with Al_2O_3 (wt%) and negatively with Fe_2O_3 (wt%), linking them to aluminosilicate phases (Figs. 7–9). Although no residual heavy minerals were directly observed in this study, earlier petrographic analyses of the flysch host rocks (Korolija et al. 1968) reported zircon, tourmaline, rutile, and apatite. These minerals, once released by mechanical weathering, likely acted as sinks for immobile elements. This is consistent with the very high Zr concentrations measured in distal lowland soils, up to approximately 400 ppm (Osekovo, sample OS-1; Supplementary Table S2).

(6) Rare earth elements

Rare earth elements (REE), together with Y and Sc, are also depleted compared to UCC (135 ppm; Rudnick & Gao 2003). TG and PG primary ores typically range from 35 to 120 ppm, while TG secondary ores are slightly higher (75–140 ppm). PG primary ores are the lowest, with a median of approximately 80 ppm. In contrast, distal lowland ores are enriched, with a median close to 300 ppm.

Correlations show that REE and Y are associated with aluminosilicates: they correlate positively with Al_2O_3 and negatively with Fe_2O_3 (Figs. 8, 9). This supports an aluminosilicate control on REE distribution. Other potential hosts appear less significant. Phosphate minerals are unlikely, as lowland ores contain little P_2O_5 (~0.2 wt%). Carbonate contents (0.4, 0.6, and 10.2 wt% CaO) show opposite trends relative to ΣREE. Earlier studies (Korolija et al. 1968) identified apatite in residual flysch fractions, and REE in soils are generally known to occur in phosphate, carbonate, or aluminosilicate phases (Tyler 2004; Ramos et al. 2016). However, in the TG–PG system, the higher Al_2O_3 content of distal lowland ores (12.5–14 wt%) compared to TG and PG primary/secondary ores (Supplementary Tables S2, S3) strongly suggests that aluminosilicates are the dominant REE carriers.

Chemical Index of Alteration

The PG and TG mineralisation is hosted within Permo-Carboniferous flysch sediments, subsequently affected by varying degrees of chemical weathering. Feldspar and carbonate minerals (except siderite) are absent in both primary and secondary mineralisation. XRD analyses indicate illite–kaolinite–chlorite mixtures (Table 2), with illite (and muscovite) dominating the matrix of the host rocks.

CIA values for TG and PG primary ores are consistently high, with medians around 85 %. TG samples display a middle 50 % range of 75–90 %, while PG values are more narrowly distributed (Fig. 11). Distal lowland secondary ores are more variable (40–85 %), reflecting the heterogeneous composition of adjacent soils. On the Al_2O_3–(CaO+Na_2O)–K_2O ternary diagram, most samples plot near the Al_2O_3 apex, consistent with advanced loss of Ca^{2+}, Na^+, and K^+ and a weathering path along the kaolinite-to-illite trend.

The kaolinite-to-illite transformation is typically associated with diagenetic conditions of approximately 90–95 °C and burial depths of 3–4 km, driven by high K^+/H^+ activity (Berger et al. 1995; Lanson et al. 2001). In the TG–PG system, this reaction required an external source of potassium:

$$Al_2Si_2O_5(OH)_4\ (\text{kaolinite}) + K^+ \rightarrow KAl_3Si_3O_{10}(OH)_2\ (\text{illite}) + 2H^+ + 3H_2O$$

Leachate analyses from siderite, baryte, and quartz (Borojević Šoštarić et al. 2009) confirm that Na^+, Ca^{2+}, Mg^{2+}, and K^+ dominated the ore-fluid system. Bulk-rock chemistry (Supplementary Table S2) shows strong depletion of Na and Ca (Na_2O<0.2 wt%; CaO<0.4 wt%), while about one third of samples are enriched in K (>1 wt% K_2O). This indicates that potassium was externally introduced during hydrothermal illitisation.

Micropetrography further supports this interpretation: host-rock matrices and veinlet infills are dominated by a sericite–quartz–siderite–opaque assemblage, consistent with hydrothermal overprinting of the flysch sediments.

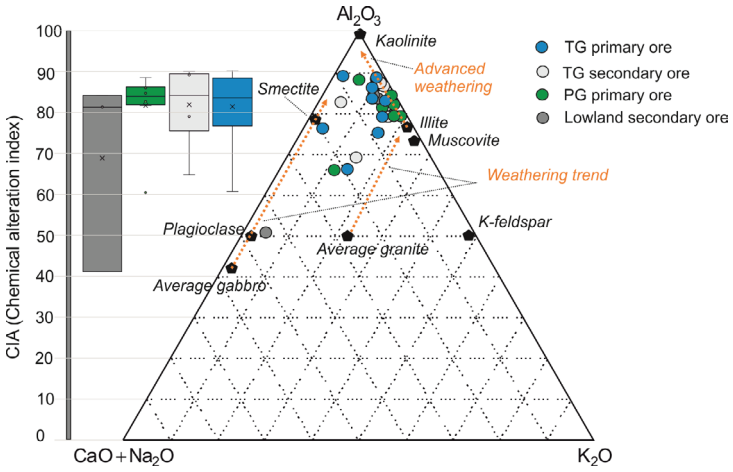

Fig. 11. The Chemical Index of Alteration (CIA) for TG primary and secondary, PG primary and lowland secondary ore calculated after Nesbitt & Young (1982, 1984). Data taken from Supplementary Table S2. See text for discussion.

The model for origin of secondary mineralisation in TG and PG region

The mineralisation at TG and PG records a three-stage evolution driven by weathering, transport, and groundwater circulation (Fig. 12; adapted after Velasco et al. 2013).

Stage 1 – Chemical weathering and oxidation

Once exposed by regional erosion, the siderite–quartz–baryte ore with minor sulphides and sulphosalts (Cu, Pb, Zn, Ag, Co, Ni, Sn, Sb, As) was rapidly altered under oxidising conditions (Fig. 12A). Pyrite and chalcopyrite dissolved through reactions with O_2 and H_2O, accelerated by Fe^{3+} and iron-oxidising bacteria such as *Gallionella ferruginea* (Ehrlich 1998; Eggerichs et al. 2019) active in moderately acid environment (pH 3–5; sensu Kisková et al. 2018). Moderately acid environment is to be expected due to presence of carbonate intercalations within flysch sequence

In this environment, goethite and limonite became the dominant alteration products, with minor malachite, azurite, and anglesite also forming (Jurković 1959, 1962, 1988; Jurković & Durn 1988). Traces of chalcocite and covellite at deeper levels suggest copper leaching and reprecipitation below the water table. As more than a third of the original iron was bound in siderite and ankerite, the resulting oxides constitute what may be described as residual or proximal gossans. Their REE and trace element signatures provide the reference against which later weathering stages can be compared (Fig. 12A).

Stage 2 – Mechanical weathering and transport

The replacement of carbonates and sulphides by secondary oxides was accompanied by significant changes in unit cell volumes, from the shrinkage of siderite to goethite to the expansion associated with haematite. This alternation between contraction and swelling induced fracturing and porosity (Figs. 4E, F, 5F, 7D), making the ore mechanically unstable. Fragmentation and downslope transport carried material into soil profiles (Majdan locality, Fig. 2A) and valley bottoms, where further alteration proceeded under variable redox conditions (Fig. 12B).

These eroded, laterally displaced accumulations of secondary iron ore are best described as distal, false (non in-situ), transported, or pedogenic gossans (sensu Velasco et al. 2013; Raines et al. 1985).While their trace element chemistry retains the imprint of the primary source, more advanced oxidative weathering is evident, including a positive Eu anomaly and a negative Ce anomaly (Zhang & Shields 2022).

Stage 3 – Groundwater transport and reprecipitation

In parallel, dissolution of iron- and base metal-bearing phases supplied Fe^{2+}, Mn^{2+}, Cu^{2+}, and Pb^{2+} into reducing groundwater, enabling migration over considerable distances. Unlike the coarse fragments redistributed by erosion, petrography of soil nodules (Fig. 6) reveals no detrital remnants of gossan, but instead textures of fresh Fe precipitation from groundwater in the vadose zone, a process characteristic of bog iron ores, as reported in Podravina region (Brenko et al. 2020, 2021).

Distal mineralisation thus represents a final stage, where the chemical mobility of Fe and Mn dominates over mechanical transport. Their REE and trace element patterns link them to the primary mineralisation and its gossan derivatives (Fig. 12C), although the signature is muted by the high aluminosilicate content inherited from weathered flysch. In contrast, enrichment in base metals is subdued, suggesting that their mobility and fixation pathways during late-stage weathering remain poorly constrained.

How far can we trace regional geochemical signature?

The geochemical signal of a region can persist for hundreds of kilometres downstream, depending on weathering intensity, climate, geomorphology, and the nature of host rocks and ores (Salminen 2005). The Trgovska (TG) and Petrova Gora (PG) area is characterised by hilly terrain, mostly below 400 m a.s.l., and a temperate humid climate with hot summers, regular rainfall, and periods of frost. These conditions have fostered a well-developed dendritic drainage network, indicative of prolonged exogenic processes. Numerous rivers and streams, including Pecka, Perna, Radonja, Glina, Žrnovnica, and Javošnica, descend from 300–140 m a.s.l., carving erosional valleys that facilitate material transport.

The central parts of TG and PG are underlain by Permian–Carboniferous flysch sediments that host primary hydrothermal Fe–(Cu, Pb) mineralisation within siltites, clayey siltstones, shales, subgreywacke sandstones, and fine-grained

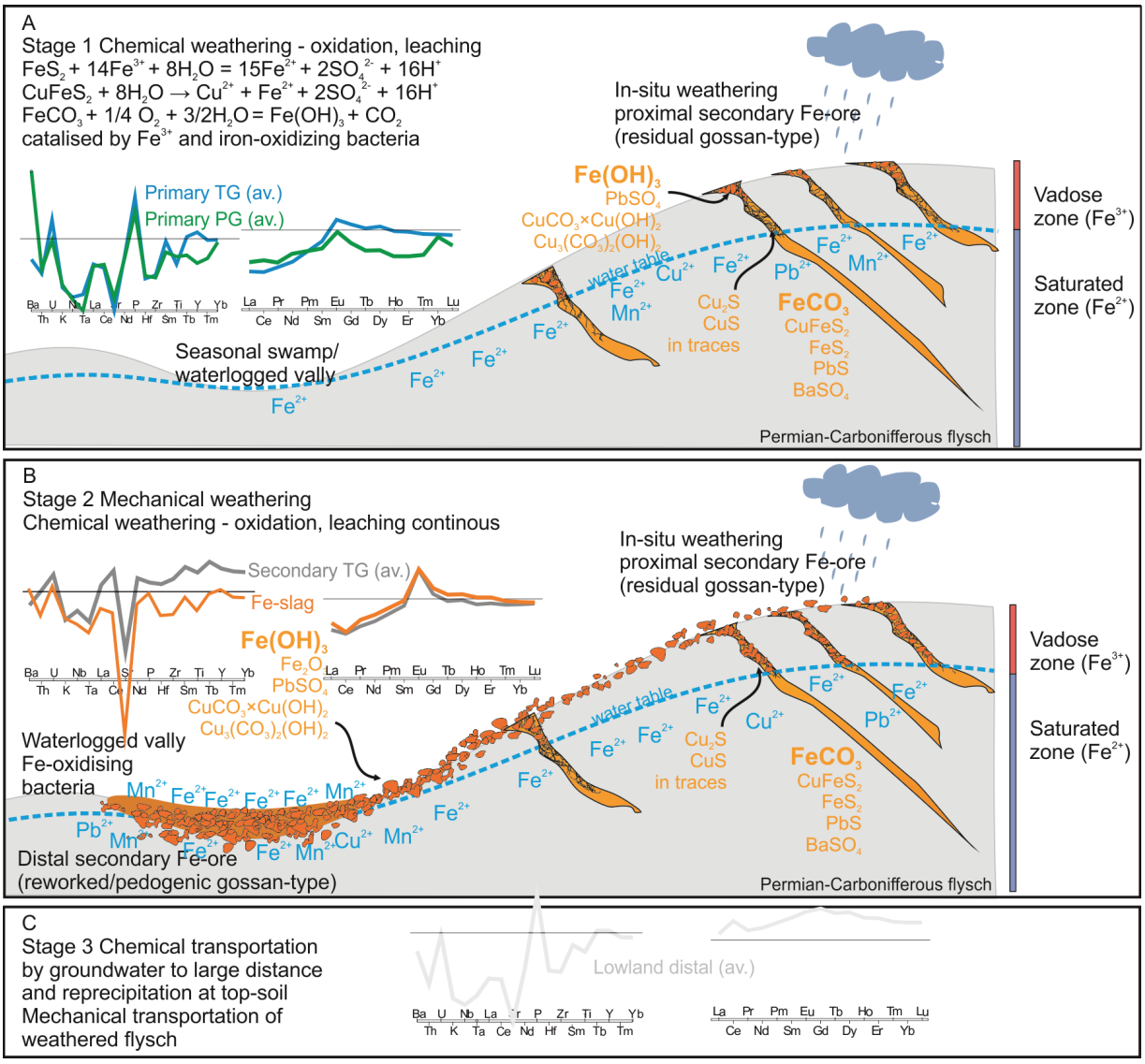

Fig. 12. Three stage evolution of the TG and PG primary and secondary mineralisation (after Velasco et al. 2013). **(A)** Stage 1 – Chemical weathering and oxidation; **(B)** Stage 2 – Mechanical weathering and transportation; **(C)** Stage 3 – Chemical transportation by groundwater to large distances and reprecipitation in topsoil. See text for discussion.

conglomerates, overlain by soils and thick vegetation. Geomorphological studies indicate variable erosion rates, with approximately 6 % of the area affected by moderate to very high erosion (Mikašinović 2018; Vrdoljak 2022; Luburić 2022). Most primary and proximal secondary Fe-ore localities (nine out of ten) are situated above 200 m a.s.l., often near the upper slopes of denuded hills, with three exceeding 300 m a.s.l.

These topographic and climatic factors enhance mechanical weathering and mobilise primary and secondary ores, facilitating their downstream transport and deposition. As a result, the regional geochemical signature of TG and PG mineralisation can be traced into lowland areas, with mechanical redeposition acting as a key factor in preserving elemental patterns away from their primary sources.

Implications for archaeological provenance studies

Provenance studies of waste from iron production (slag) or iron semi-products and objects (slag inclusions) are based on the observation of rare earth elements and immobile trace elements (Benvenuti et al. 2000, 2013; Schwab et al. 2006; Desaulty et al. 2008) and isotope analyses (Milot et al. 2016; Rose et al. 2019). As the present example shows, the geochemical signature can trace primary and secondary mineralisation (proximal and distal; Fig 12B) and even distal incipient bog iron ores, which means that the signature covers an entire region, spatially distant and distinctly different areas (mountainous and lowland). This in turn leaves archaeologically significant questions related to ore sourcing strategies, the organisation of iron production workflows, connectivity

and distribution networks of raw materials, semi-finished and finished products, tangible in a very broad sense – at a broad regional level. The results of this study highlight the importance of a comprehensive geological analysis of the ores and their paragenesis in order to obtain more detailed provenance data that will allow a more precise localisation of the ore sources. By comparing slag sample with samples of primary and secondary mineralisation from a unique site (Jokin Potok) and samples in a larger regional framework, it is possible to define the highest correlation to a unique ore type and spatially delineate more precisely the potential mining areas (Figs. 8, 9; sample JP 4). In particular, there is a clear correlation in the anomalous representation of REE (Eu, Ce), indicating chemical weathering under oxidising conditions of primary hydrothermal mineralisation, and linking the slag more closely to its source ore – secondarily mineralised, either proximal/residual gossan or distal reworked/pedogenic gossan, present here in the form of limonite/goethite with the highest iron content of all ores analysed. In addition, a relative contribution to the localisation of the ore sources in this case is the enrichment of MnO, which is characteristic of the region, but is more pronounced on the Trgovska gora Mt within the analysed samples, specifically at the location where the slag was found, as well as at other spatially quite close locations.

Conclusion

The Petrova and Trgovska Gora massifs preserve a distinct regional geochemical fingerprint that can be traced from primary ore, through proximal secondary gossans, to incipient bog-iron deposits more than 100 km away. This signature is defined by immobile trace elements, REE, redox-sensitive metals, Fe–Mn, and base metals associated with primary mineralisation.

Primary and proximal secondary ores are shaped by three key factors:

- Host rock composition – flysch-derived aluminosilicates (illite–kaolinite–chlorite mixtures, residual zircon, tourmaline, rutile, apatite) impart characteristic depletions in immobile elements (Zr, Nb, Ta, Hf, W, REE, Sc, Y) and enrichments in redox-sensitive elements (Mo, V, U) relative to the upper continental crust (UCC).
- Primary mineralisation – enrichment in Fe (30–75 wt% Fe_2O_3), Mn, and base metals (Cu, Pb, Zn, Ag, Co, Ni, Sn, Sb, As), along with Ba and S, marks the initial ore composition.
- Secondary weathering – further Mn and base metal enrichment, coupled with negative Ce and positive Eu–Yb anomalies, reflects advanced alteration. High CIA values (~85 %) indicate intense chemical weathering and alkali loss, with illitisation likely driven by hydrothermal processes, later enhanced by low-pH secondary weathering.

Distal lowland deposits display lower Fe contents (median ~15 wt% Fe_2O_3) but elevated base metal and immobile element concentrations. Their enrichment patterns reflect both the mechanical transport of flysch detritus and the chemical redistribution of metals during pedogenic and bog-iron formation.

The weathering history can be summarised in three stages:

- Proximal alteration (gossan formation) – oxidation of siderite–polysulphide assemblages under acidic (pH 2–3.5) conditions produces goethite, limonite, malachite, azurite, and anglesite in the vadose zone, with minor covellite and chalcocite in the saturated zone.
- Distal reworking – mechanical erosion and downslope transport of weathered Fe ores lead to deposition in soil profiles, valleys, and seasonal swamps as reworked or pedogenic gossans. Oxidation-driven volume changes facilitate ore disintegration.
- Regional redistribution – long-distance transport of dissolved Fe^{2+}, Mn^{2+}, and trace metals by reducing groundwater, followed by reprecipitation in topsoils, results in the formation of bog-iron ores. Mechanical erosion of flysch and gossan fragments occurs in parallel, mediated by streams and rivers.

This work also propose a methodological framework for geoarchaeological provenance studies: (i) immobile trace elements and REE reliably distinguish primary, secondary, and distal bog-iron deposits, serving as regional markers; (ii) bulk chemistry and multivariate analysis enable intra-regional discrimination at ore type and deposit levels; (iii) ΣREE values and Ce–Eu anomalies preserved in slag, not altered by exogenic pollution during direct reduction, offering insights into ore evolution stages and narrowing source attribution; (iv) redox-sensitive elements (Mo, V, U, Th) provide further discrimination of ore types and weathering stages; U and Th, in particular, are minimally altered during smelting, making them especially robust tracers.

In sum, the study demonstrates that geochemical fingerprints can be tracked from primary carbonate replacement mineralisation through weathering and transport to distal bog-iron deposits. This integrated approach strengthens interpretations of past metallurgical supply networks and provides a transferable framework for provenance research in geoarchaeology.

Acknowledgements: This work was supported by KulturFER project (HRZZ IP-2022-10-1846) “Cultural Landscapes of Iron Metallurgy During Antiquity and the Early Middle Ages in the Sava and Drava River Basin”, funded by the Croatian Science foundation; “Synergy of Diversity: Archaeology of Landscape and Technological Traditions in Continental and Adriatic Croatia (SirAkt)”, funded by the European Union-NextGenerationEU and the Virtulab project (KK.01.1.1.02.0022), co-funded by the European Regional Development Fund.

References

Andrew R.L. 1984: The geochemistry of selected base-metal gossans, Southern Africa. *Journal of Geochemical Exploration* 22, 161–192.

Barbieri M., Masi U. & Tolomeo L. 1982: Strontium geochemistry in the epithermal barite deposits from the Apuan Alps (northern Tuscany, Italy). *Chemical Geology* 35, 351–356. https://doi.org/10.1016/0009-2541(82)90011-0

Bennett W.W. & Canfield D.E. 2020: Redox-sensitive trace metals as paleoredox proxies: A review and analysis of data from modern sediments. *Earth Science Reviews* 204, 103175. https://doi.org/10.1016/j.earscirev.2020.103175

Benvenuti M., Mascaro I., Costagliola P., Tanelli G. & Romualdi A. 2000: Iron, copper and tin at Baratti (Populonia): smelting processes and metal provenances. *Journal of the Historical Metallurgy Society* 34, 67–76.

Benvenuti M., Dini A., D'Orazio M., Chiarantini L., Corretti A. & Costagliola P. 2013: The tungsten and tin signature of iron ores from Elba Island (Italy): a tool for provenance studies of iron production in the Mediterranean region. *Archaeometry* 55, 479–506. https://doi.org/10.1111/j.1475-4754.2012.00692.x

Berger G., Beaufort D. & Lacharpagne J.-C. 1995: Dissolution of sanidine up to 300 °C near equilibrium at approximately neutral pH. In: Arehart G.B. & Hultson J.R. (eds.): Water-Interaction. *Balkema*, Rotterdam, 823–826.

Blain C.F. & Andrew R.L. 1977: Sulfide weathering and the evaluation of gossans in mineral exploration. *Minerals Science and Engineering* 9, 119–150.

Boch R., Wang X., Kluge T. & Dietzel M. 2018: Aragonite–calcite veins of the 'Erzberg' iron ore deposit (Austria): Environmental implications from young fractures. *Sedimentology* 66, 604–635. https://doi.org/10.1111/sed.12500

Boláček O. & Mihok J. 1994: Present day conditions and future of mining of siderite deposit Nižna Slana. *Mineralia Slovaca* 26, 1–4 (in Slovak).

Borojević Šoštarić S., Palinkaš L.A., Strmić Palinkaš S., Bermanec V., Neubauer F., Spangenberg J. & Prochaska W. 2009: Origin of siderite mineralisations in Petrova and Trgovska Gora Mts., NW Dinarides. *Mineralogy and Petrology* 97, 111–128. https://doi.org/10.1007/s00710-009-0055-1

Borojević Šoštarić S., Neubauer F., Handler R. & Palinkaš L.A. 2012: Tectonothermal history of the basement rocks within NW Dinarides: new $^{40}Ar/^{39}Ar$ ages and synthesis. *Geologica Carpathica* 63, 441–452. https://doi.org/10.2478/v10096-012-0036-4

Borojević Šoštarić S., Roglić M., Milošević A. & Brenko T. 2022: Žune Ba–F epithermal deposit. Part 1: Mineralogical and geochemical characteristics. *Geologia Croatica* 75, 393–410. https://doi.org/10.4154/gc.2022.32

Boyle D.R. 1994: Oxidation of massive sulfide deposits in the Bathurst mining camp, New Brunswick – Natural analogs for acid drainage in temperate climates. In: Alpers C.N. & Blowes D.W. (eds.): Environmental Geochemistry of Sulfide Oxidation. *ACS Symp. Series* 550, 535–550.

Brenko T., Šoštarić S.B., Ružičić S. & Ivančan T.S. 2020: Evidence for the formation of bog iron ore in soils of the Podravina region, NE Croatia: Geochemical and mineralogical study. *Quaternary International* 536, 13–29. https://doi.org/10.1016/j.quaint.2019.10.010

Brenko T., Šoštarić S.B., Karavidović T., Ružičić S. & Ivančan T.S. 2021: Geochemical and mineralogical correlations between the bog iron ores and roasted iron ores of the Podravina region, Croatia. *Catena* 204, 105353. https://doi.org/10.1016/j.catena.2021.105353

Butt C.R.M. & Zeegers H. 1992: Regolith Exploration Geochemistry in Tropical and Subtropical Terrains. *Elsevier*, Amsterdam.

Butt C.R.M., Robertson D.M., Scott K.M. & Cornelius M. 2005: Regolith Expression of Australian Ore Systems. *CSIRO Publishing*, Collingwood.

Butt C.R.M., Scott K.M., Cornelius M. & Robertson D.M. 2008: Regolith sampling for geochemical exploration. In: Scott K.M. & Pain C.F. (eds.): Regolith Science. *Springer and CSIRO Publishing*, Dordrecht/Collingwood, 341–376.

Desaulty A.M., Mariet C., Dillmann P., Joron J.L. & Fluzin P. 2008: A provenance study of iron archaeological artefacts by inductively coupled plasma–mass spectrometry multi-elemental analysis. *Spectrochimica Acta B* 63, 1253–1262. https://doi.org/10.1016/j.sab.2008.08.017Đurđanović Ž. 1968: Conodonten des Unterdevons und Unterkarbons westlich von Dvor na Uni (Kroatien-Jugoslawien). *Geološki Vjesnik* 21, 83–103.

Đurđanović Ž. 1973: About the Palaeozoic and the Triassic of Medvednica Mountain and the area near Dvor na Uni on the basis of Conodonts. *Geološki Vjesnik* 25, 29–51.

Durman A. 2002: Iron resources and production for the Roman frontier in Pannonia. *Journal of the Historical Metallurgy Society* 36, 24–32.

Eggerichs T., Wiegand M., Neumann K., Opel O., Thronicker O. & Szewzyk U. 2019: Growth of iron-oxidizing bacteria Gallionella ferruginea and Leptothrix cholodnii in oligotrophic environments. *Geomicrobiological Journal* 37, 190–199. https://doi.org/10.1080/01490451.2019.1686667

Ehrlich H.L. 1998: Geomicrobiology: its significance for geology. *Earth Science Reviews* 45, 45–60. https://doi.org/10.1016/S0012-8252(98)00034-8

Emmons W.H. 1917: The Enrichment of Ore Deposits. *U.S. Geological Survey Bulletin* 625, 1–530.

Faryad S. & Hoinkes G. 2003: P–T gradient of Eo-Alpine metamorphism within the Austroalpine basement units east of the Tauern Window (Austria). *Mineralogy and Petrology* 77, 129–159. https://doi.org/10.1007/s00710-002-0196-1

Goldberg S., Forster H. S. & Godfrey C. L. 1996: Molybdenum Adsorption on Oxides, Clay Minerals, and Soils. *Advances in Agronomy* 56, 67–129. https://doi.org/10.2136/sssaj1996.03615995006000020013x

Hofstra A.H., Korpás L., Csalagovits I., Johnson C.A. & Christiansen W.D. 1999: Stable isotopic study of the Rudabánya iron mine. A carbonate-hosted siderite, barite, base metal sulphide replacement deposit. *Geologica Hungarica, Series Geologica* 24, 295–302.

Hrvatović H. 2000: Paleozoic of Mid-Bosnian Schist Mountains (MBSM). In: Pamić J. & Tomljenović B. (eds.): Pancardi 2000 Fieldtrip Guidebook. *Vijesti HGD* 37, 75–77.

Hrvatović H. & Pamić J. 2005: Principal thrust-nappe structures of the Dinarides. *Acta Geologica Hungarica* 48, 133–151. https://doi.org/10.1556/ageol.48.2005.2.4

Hurai V., Harcová E., Huraiová M., Ozdín D., Prochaska W. & Wiegerová V. 2002: Origin of siderite veins in the Western Carpathians I. P–T–X– $\delta^{13}C$–$\delta^{18}O$ relationship in ore-forming brines of the Rudňany deposits. *Ore Geology Reviews* 21, 67–101.

Jacobsen S.D., Smyth J.R., Swope R.J. & Downs R.T. 1998: Rigid-body character of the SO_4 groups in celestine, anglesite and barite. *Canadian Mineralogist* 36, 1053–1060.

Jurković I. 1958: Metalogeny of Petrova Gora Mt. in southwestern Croatia. *Geološki Vjesnik* 11, 143–228.

Jurković I. 1959: Polymetal paragenesis of the ore occurrence near Dvor na Uni. *Geološki Vjesnik* 13, 149–161.

Jurković I. 1962: The results of ore deposit research in Croatia. *Geološki Vjesnik* 15, 249–294.

Jurković I. 1988: The Hercynian metallogenesis of the ore deposits of Trgovska Gora in Croatia. *Geološki Vjesnik* 41, 369–393.

Jurković I. & Durn G. 1988: Lead deposit in the Zrin District of Trgovska Gora in Croatia. *Geološki Vjesnik* 41, 317–339.

Jurković I., Garašić V. & Hrvatović H. 2010: Geochemical characteristics of the barite occurrences in southeastern Bosnia. *Geologia Croatica* 63, 241–258. https://doi.org/10.4154/gc.2010.20

Karavidović T. & Brenko T. 2022: Nature of the deposit and properties of bog iron ore at the Kalinovac–Hrastova Greda: A model

for the analysis of ore exploitation and use in archaeological periods. *Prilozi Instituta za arheologiju u Zagrebu* 39, 219–261. https://doi.org/10.33254/piaz.39.2.5

Karavidović T. & Drnić I. 2022: Traces of iron production in Donje Pokuplje in the 1st millennium BC. In: Sekelj Ivančan T. & Karavidović T. (eds.): Secrets of Iron – From Raw Material to an Iron Object. Proceedings of the 7th International Conference of Mediaeval Archaeology. *Institut za arheologiju*, Zagreb, 87–112.

Kisková J., Perháčová Z., Vlčko L. et al. 2018: The Bacterial Population of Neutral Mine Drainage Water of Elizabeth's Shaft (Slovinky, Slovakia). *Current Microbiology* 75, 988–996. https://doi.org/10.1007/s00284-018-1472-6

Klein C. 2003: The 22nd Edition of the Manual of Mineral Science. *John Wiley & Sons*, New York & Chichester, xii + 644 pp. + CD-ROM.

Korolija B., Živaljević T. & Šimunić A.N. 1968: Explanatory notes for the Basic Geological Map of SFRJ 1:100,000, Slunj sheet (in Croatian). *Federal Geological Survey*, Belgrade, 1–44.

Korolija B., Živaljević T. & Šimunić A. 1981: Explanatory notes for the geological map 1:100,000, sheet Slunj. *Geological Survey*, Belgrade.

Lanson B., Beaufort D., Berger G., Bauer A., Cassagnabere A. & Meunier A. 2001: Authigenic kaolin and illitic minerals during burial diagenesis of sandstones: A review. *Clay Minerals* 37, 1–22. https://doi.org/10.1180/0009855023710014

Luburić F. 2022: Assessment of soil erosion in the Banovina area using the RUSLE method. *M.Sc. thesis, University of Zagreb*, 1–70. https://repozitorij.rgn.unizg.hr/islandora/object/rgn:2367

Marković S. 2002: Hrvatske mineralne sirovine. *Institut za geološka istraživanja, Zavod za geologiju*, Zagreb, 1–544.

Mikašinović M. 2018: Morphometric analysis of relief of Petrova gora. *M.Sc. thesis, University of Zagreb*, 1–48. https://repozitorij.pmf.unizg.hr/islandora/object/pmf:4689

Milot J., Poitrasson F., Baron S. & Coustures M.P. 2016: Iron isotopes as a potential tool for ancient iron metals tracing. *Journal of Archaeological Science* 76, 9–20. https://doi.org/10.1016/j.jas.2016.10.003

Németh N., Földessy J. & Turi J. 2017: Ore geology of the copper sulfide mineralisation in the Rudabánya ore-bearing complex. *Central European Geology* 60, 53–72. https://doi.org/10.1556/24.59.2016.005

Nesbitt H.W. & Young G.M. 1982: Early Proterozoic climates and plate motions inferred from major element chemistry of lutites. *Nature* 299, 715–717. https://doi.org/10.1038/299715a0

Nesbitt H.W. & Young G.M. 1984: Prediction of some weathering trends of plutonic and volcanic rocks based on thermodynamic and kinetic considerations. *Geochimica et Cosmochimica Acta* 48, 1523–1534. https://doi.org/10.1016/0016-7037(84)90407-0

Neubauer F., Liu Y., Chang R. & Guan Q. 2025: U–Pb zircon ages constrain the Miocene age of hydrothermal activity in the iron mining Hüttenberg-Waitschach district (Austria), faulting and landscape evolution in the Eastern Alps. *International Journal of Earth Sciences* 114. https://doi.org/10.1007/s00531-025-02512-3

Orucoglu E., Grangeon S., Gloter A., Robinet J.-C., Madé B. & Tournassat C. 2022: Competitive adsorption processes at clay mineral surfaces: A coupled experimental and modeling approach. *ACS Earth Space Chemistry* 6, 144–159. https://doi.org/10.1021/acsearthspacechem.1c00323

Palinkaš L.A. & Jurković I. 1994: Lanthanide geochemistry and fluid inclusion peculiarities of fluorite from the barite deposits south of Kreševo (Bosnia and Herzegovina). *Geologia Croatica* 47, 103–115. https://doi.org/10.4154/gc.1994.10

Palinkaš L.A., Borojević Šoštarić S. & Strmić Palinkaš S. 2008: Metallogeny of the northwestern and central Dinarides and southern Tisia. *Ore Geology Reviews* 34, 501–520. https://doi.org/10.1016/j.oregeorev.2008.05.006

Palinkaš L.A., Borojević Šoštarić S., Strmić Palinkaš S., Prochaska W., Pécskay Z., Neubauer F. & Spangenberg J.E. 2016: The Ljubija geothermal field: A herald of the Pangea break-up (NW Bosnia and Herzegovina). *Geologia Croatica* 69, 3–30. https://doi.org/10.4154/GC.2016.02

Pan Y. & Fleet M.E. 1992: Mineral chemistry and geochemistry of vanadian silicates in the Hemlo gold deposit, Ontario, Canada. *Contributions to Mineralogy and Petrology* 109, 511–525. https://doi.org/10.1007/BF00306553

Pfingstl S., Kurz W., Schuster R. & Hauzenberger C. 2015: Geochronological constraints on the exhumation of the Austroalpine Seckau Nappe (Eastern Alps). *Austrian Journal of Earth Sciences* 108, 172–185. https://doi.org/10.17738/ajes.2015.0011

Prochaska W. 2016: Genetic concepts on the formation of the Austrian magnesite and siderite mineralisations in the Eastern Alps of Austria. *Geologia Croatica* 69, 31–38. https://doi.org/10.4154/GC.2016.03

Radvanec M., Grecula P. & Žák K. 2004: Siderite mineralisation of the Gemericum superunit (Western Carpathians, Slovakia): review and a revised genetic model. *Ore Geology Reviews* 24, 267–298.

Raines G.L., McGee L.G. & Sutley S.J. 1985: Near-infrared spectra of West Shasta gossans compared with true and false gossans from Australia and Saudi Arabia. *Economic Geology* 80, 8, 2230–2239. https://doi.org/10.2113/gsecongeo.80.8.2230

Ramos S.J., Dinali G.S., Oliveira C., Martins G.C., Moreira C.G., Siqueira J.O. & Guilherme L.R.G. 2016: Rare earth elements in the soil environment. *Current Pollution Reports* 2, 28–50. https://doi.org/10.1007/s40726-016-0026-4

Rose T., Télouk P., Klein S. & Marschall H.R. 2019: Questioning Fe isotopes as a provenance tool: Insights from bog iron ores and alternative applications in archaeometry. *Journal of Archaeological Science* 101, 52–62. https://doi.org/10.1016/j.jas.2018.11.005

Rudnick R.L. & Gao S. 2003: The composition of the continental crust. In: Holland H.D. & Turekian K.K. (eds.): Treatise on Geochemistry, vol. 3. *Elsevier-Pergamon*, Oxford, 1–64. https://doi.org/10.1016/B0-08-043751-6/03016-4

Salminen R. 2005: Geochemical Atlas of Europe. Part 1: Background Information, Methodology and Maps. *Geological Survey of Finland*, Espoo, 1–526.

Schmid S.M., Fügenschuh B., Kounov A., Matenco L., Nievergelt P., Oberhänsli R., Pleuger J., Schefer S., Schuster R., Tomljenović B., Ustaszewski K. & van Hinsbergen D.J.J. 2020: Tectonic units of the Alpine collision zone between Eastern Alps and western Turkey. *Gondwana Research* 78, 308–374. https://doi.org/10.1016/j.gr.2019.07.005

Schulz O. & Schroll E. 1997: Sideritbezirk Hüttenberg. In: Weber L. (Ed.): Handbuch der Lagerstätten der Erze, Industrieminerale und Energierohstoffe Österreichs: Erläuterungen zur metallogenetischen Karte von Österreich 1:500 000 unter Einbeziehung der Industrieminerale und Energierohstoffe, 19. *Geologische Bundesanstalt*, 291–293.

Schwab R., Heger D., Höppner B. & Pernicka E. 2006: The provenance of iron artefacts from Manching: A multi-technique approach. *Archaeometry* 48, 433–452. https://doi.org/10.1111/j.1475-4754.2006.00265.x

Sherman D.M., Hubbard C.G. & Peacock C.L. 2008: Surface complexation of U(VI) by Fe and Mn (hydr)oxides. In: Merkel B.J. & Hasche-Berger A. (eds.): Uranium, Mining and Hydrogeology. *Springer*, Berlin, Heidelberg. https://doi.org/10.1007/978-3-540-87746-2_122

Šikić K., Basch O. & Šimunić A. 1979: Tumač osnovne geološke karte 1:100,000, list Zagreb [Basic Geological Map of the Republic of Croatia 1:100,000, explanatory notes for Zagreb sheet]. *Savezni geološki zavod*, Beograd, 1–81 (in Croatian).

Strmić Palinkaš S., Spangenberg J.E. & Palinkaš L.A. 2009: Organic and inorganic geochemistry of Ljubija siderite deposits, NW Bosnia and Herzegovina. *Mineralium Deposita* 44, 893–913. https://doi.org/10.1007/s00126-009-0249-z

Taylor G.F. & Thornber M.R. 1992: Gossan and ironstone surveys. In: Butt C.R.M. & Zeegers H. (eds.): Regolith Exploration Geochemistry in Tropical and Subtropical Terranes. *Handbook of Exploration Geochemistry* 4, *Elsevier*, Amsterdam, 139–202.

Taylor G.F., Wilmshurst J.R., Butt C.R.M. & Smith R.E. 1980: Gossans. *Journal of Geochemical Exploration* 22, 30–32.

Taylor S.R. & McLennan S.M. 1995: The geochemical evolution of the continental crust. *Reviews of Geophysics* 33, 241–265. https://doi.org/10.1029/95RG00262

Thelemann M., Bebermeier W., Hoelzmann P. & Lehnhardt E. 2017: Bog iron ore as a resource for prehistoric iron production in Central Europe: A case study of the Widawa catchment area in eastern Silesia, Poland. *Catena* 149, 474–490. https://doi.org/10.1016/j.catena.2016.04.002

Thornber M.R. 1985: Supergene alteration of sulfides: VII. Distribution of elements during the gossan-forming process. *Chemical Geology* 53, 279–301.

Tribovillard N., Algeo T.J., Lyons T. & Riboulleau A. 2006: Trace metals as paleoredox and paleoproductivity proxies: An update. *Chemical Geology* 232, 12–32. https://doi.org/10.1016/j.chemgeo.2006.02.012

Tyler G. 2004: Rare earth elements in soil and plant systems – A review. *Plant and Soil* 267, 191–206. https://doi.org/10.1007/s11104-005-4888-2

Vaitkus A., Merkys A., Sander T., Quirós M., Thiessen P.A., Bolton E.E. & Gražulis S. 2023: A workflow for deriving chemical entities from crystallographic data and its application to the Crystallography Open Database. *Journal of Cheminformatics* 15, 123. https://doi.org/10.1186/s13321-023-00780-2

Velasco F., Herrero J.M., Suárez S., Yusta I., Alvaro A. & Tornos F. 2013: Supergene features and evolution of gossans capping massive sulphide deposits in the Iberian Pyrite Belt. *Ore Geology Reviews* 53, 181–203. https://doi.org/10.1016/j.oregeorev.2013.01.008

Velić I. & Vlahović I. 2009: Tumač geološke karte 1:300,000 [Basic Geological Map of the Republic of Croatia 1:300,000, explanatory notes – in Croatian]. *Croatian Geological Survey*, Zagreb, 1–147.

Vrdoljak S. 2022: Morphometric analysis of rivers Utinja, Glina & Petrinjčica based on digital elevation model. *M.Sc. thesis, University of Zagreb*, 1–61 (in Croatian with English summary). https://repozitorij.rgn.unizg.hr/islandora/object/rgn:2123/datastream/PDF/download (accessed 19 December 2024)

Weber J., Barthel J., Brandt F., Klinkenberg M., Breuer U., Kruth M. & Bosbach D. 2016: Nano-structural features of barite crystals observed by electron microscopy and atom probe tomography. *Chemical Geology* 424, 51–59.

Zhang K. & Shields G. A. 2022: Sedimentary Ce anomalies: Secular change and implications for paleoenvironmental evolution. *Earth-Science Reviews* 229, 104015. https://doi.org/10.1016/j.earscirev.2022.104015

Electronic supplementary material is available online:
Supplementary Table S1 at https://geologicacarpathica.com/data/files/supplements/GC-77-2-Borojevic-Sostaric_TableS1.xlsx
Supplementary Table S2 at https://geologicacarpathica.com/data/files/supplements/GC-77-2-Borojevic-Sostaric_TableS2.xlsx
Supplementary Table S3 at https://geologicacarpathica.com/data/files/supplements/GC-77-2-Borojevic-Sostaric_TableS3.xlsx
Supplementary Table S4 at https://geologicacarpathica.com/data/files/supplements/GC-77-2-Borojevic-Sostaric_TableS4.xlsx